J Solid State Electrochem (2010) 14:1125–1144
DOI 10.1007/s10008-009-0932-0

REVIEW PAPER

Cathode materials for solid oxide fuel cells: a review

Chunwen Sun · Rob Hui · Justin Roller

Received: 15 June 2009 / Revised: 24 August 2009 / Accepted: 29 August 2009 / Published online: 8 October 2009

Abstract The composition and microstructure of cathode materials has a large impact on the performance of solid oxide fuel cells (SOFCs). Rational design of materials composition through controlled oxygen nonstoichiometry and defect aspects can enhance the ionic and electronic conductivities as well as the catalytic properties for oxygen reduction in the cathode. Cell performance can be further improved through microstructure optimization to extend the triple-phase boundaries. A major degradation mechanism in SOFCs is poisoning of the cathode by chromium species when chromium-containing alloys are used as the interconnect material. This article reviews recent developments in SOFC cathodes with a principal emphasis on the choice of materials. In addition, the reaction mechanism of oxygen reduction is also addressed. The development of Cr-tolerant cathodes for intermediate temperature solid oxide fuel cells, and a possible mechanism of Cr deposition at cathodes are briefly reviewed as well. Finally, this review will be concluded with some perspectives on the future of research directions in this area.

Keywords Solid oxide fuel cells · Cathode materials · Microstructure · Reaction mechanism · Chromium poisoning

Introduction

Fuel cells are devices for electrochemically converting chemical energy into electrical energy and heat without the need for direct combustion as an intermediate step, giving much higher conversion efficiencies than conventional energy systems. In particular, solid oxide fuel cells (SOFCs), based on an oxide-ion conducting electrolyte, have several advantages over other types of fuel cells, including relatively inexpensive materials, low sensitivity to impurities in the fuel, and high efficiency [1–3].

SOFCs cannot yet compete with conventional combustion systems in terms of cost and durability. In recent years, great efforts have been devoted to develop low or intermediate temperature SOFCs (IT-SOFCs) operating at 500–800 °C. Lowering the operating temperature can suppress degradation of components and extend the range of acceptable material selection; this also serves to improve cell durability and reduce the system cost. However, reducing the operating temperature decreases the electrode kinetics and results in large interfacial polarization resistances. This effect is most pronounced for the oxygen reduction reaction at the cathode. In order to lower the polarization resistance of the cathode, a favorable electronic and ionic conductivity as well as a high catalytic activity for oxygen reduction must be maintained.

A vast number of papers related to the topic of SOFC cathodes have been published in the past three decades. Regrettably, it is not possible to cover all cathode aspects and references in the literature. This review aims to provide an overview of present research progress in the field of SOFC cathodes and will focus especially on the most widely used materials and related reaction mechanisms. Further emphasis will be placed on the development of cathode materials for low and IT-SOFCs including new cathode materials and microstructure optimization.

Overview of cathode reaction mechanism

Cathode requirements

In SOFCs, the cathode functions as the site for the electrochemical reduction of oxygen. To this effect, the

C. Sun (✉) · R. Hui · J. Roller
Institute for Fuel Cell Innovation,
National Research Council Canada,
4250 Wesbrook Mall,
Vancouver, BC V6T 1W5, Canada
e-mail: Springwensun@yahoo.com.cn
e-mail: Chunwen.Sun@nrc-cnrc.gc.ca

cathode must have: (1) high electronic conductivity (preferably more than 100 S cm^{-1} under oxidizing atmosphere); (2) a matched thermal expansion coefficient (TEC) and chemical compatibility with the electrolyte and interconnect materials; (3) adequate porosity to allow gaseous oxygen to readily diffuse through the cathode to the cathode/electrolyte interface; (4) stability under an oxidizing atmosphere during fabrication and operation; (5) high catalytic activity for the oxygen reduction reaction (ORR); and (6) low cost. For high temperature SOFCs operating typically at 800–1000 °C, the cathode material of choice is a composite of Sr-doped $LaMnO_3$ (LSM) and yttria-stabilized zirconia (YSZ). Other mixed ionic-electronic conductors (MIECs) have also been used as the cathode and are discussed later.

The operating temperature of SOFCs is determined by the temperature required to achieve sufficient ionic conductivity in the electrolyte. In addition, the choice of cathode materials is largely dependent on the electrolyte materials used with care taken to match thermal expansion coefficients and avoid undesirable interface reactions. The most commonly used electrolyte material is yttria-stabilized zirconia. Other oxides, such as scandia-stabilized zirconia, samaria-doped ceria (SDC), gadolinia-doped ceria (GDC), and lanthanum strontium gallium magnesium oxide (LSGM), are also under consideration because they have higher ionic conductivities at reduced operating temperatures. Selected data on the TEC and ionic conductivity of several commonly used electrolyte materials are listed in Table 1.

Triple-phase boundaries at cathodes

On the surface of the cathode, the oxygen reduction can be described as follows:

$$\frac{1}{2}O_2(\text{gas}) + 2e^-(\text{cathode}) \rightarrow O^{2-}(\text{electrolyte}) \quad (1)$$

The electrochemical reactions are quite different from normal heterogeneous catalytic reaction in many aspects [11]. For instance, it is widely believed that the electrochemical reactions can only occur at the triple-phase boundaries (TPBs), which are defined as the confluence of sites where the oxygen ion conductor, electronic conductor, and the gas phase come in contact. A schematic illustration of the region between the electrolyte and the cathode where the TPB exists is shown in Fig. 1. If there is a breakdown in connectivity in any one of the three phases, the reaction cannot occur [12]. Furthermore, a hindrance of access for ions, gasses, or electrons to the reaction site renders it inactive. Microstructure and composition clearly affect the size and distribution of the TPBs. One compositional design option employed is to provide a single-phase electrode with mixed conductivities permitting both oxide ion and electron mobility within the cathode material, e.g., $La_{1-x}Sr_xCo_{1-y}Fe_yO_{3-\delta}$(LSCF). Thus, electrochemical oxygen reduction can occur at the electrode surface as well as within the bulk electrode. Another strategy is to use a porous composite consisting of an electronic conducting cathode material and an appropriate amount of ionic conducting electrolyte material, e.g., LSM-YSZ. By using these strategies, the electrochemically active reaction sites can be orders of magnitude greater than that of porous cathodes exhibiting only electronic conductivity. The degree of this extension depends critically on the rate of defect transport through the solid MIECs, gas transport through the pores to promote surface coverage in the MIECs, and the catalytic activity of interfaces.

Kinetics and reaction mechanisms of cathodes

Although the molecular species involved in the overall electrochemical reactions at the cathode is a single diatomic species (O_2), it must first be converted to some "electro-active" intermediate form via one or more processes. Usually, this electrochemically kinetic step is restricted to an area close to TPBs [13, 14]. The electrochemical processes going on in the cathode involve different bulk and surface steps [12, 14, 15]. The elementary reactions in the overall electrode reaction are usually considered as follows [16, 17]: (1) the reduction of O_2 molecules involving adsorption, dissociation, reduction, and incorporation of the oxygen anion into the lattice of the cathode materials; (2) ionic transport through the porous cathode toward the electrolyte; and (3) the ion jumping into the electrolyte lattice. Among all three elementary reaction steps, several steps could be rate-limiting for the oxygen reduction process. The oxygen reduction step is the biggest contributor to total cell resistance, and improvements on the

Table 1 TEC and ionic conductivity of electrolyte materials in air at 800 °C

Composition	TEC ($\times 10^{-6}K^{-1}$)	σ_i (Scm^{-1})	References
$(Y_2O_3)_{0.08}(ZrO_2)_{0.92}$	10.5	0.03	[4]
$(Sc_2O_3)_{0.08}(ZrO_2)_{0.92}$	10.7	0.13	[4]
$Ce_{0.8}Gd_{0.2}O_{1.9}$	12.5	0.053	[5, 6]
$Ce_{0.8}Sm_{0.2}O_{1.9}$	12.2	0.095	[5, 7]
$La_{0.9}Sr_{0.1}Ga_{0.8}Mg_{0.2}O_{2.85}$	10.7	0.1	[8–10]

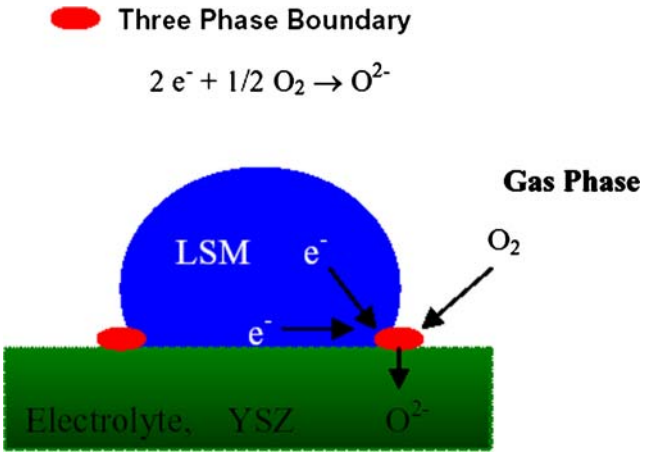

Fig. 1 Schematic diagram of the cathode triple-phase boundary

catalytic activity of the cathode have a strong impact on the final cell performance [18, 19].

For electron-conducting perovskite-type materials, Fleig [20] summarized three possible paths for the cathodic reaction (Eq. 1), that is, the electrode surface path, the bulk path, and the electrolyte surface path as shown in Fig. 2. These three paths are in sequence suitable for the cases of an electronic conductor (e.g., LSM), an MIEC conductor (e.g., LSCF), and a composite (e.g., LSM-YSZ), respectively. It should be noted here that only at higher partial pressure of oxygen (p_{O2}) that corresponds to the cathode operating conditions of SOFCs, LSM has a p-type conductivity. However, with decreasing p_{O2} and increasing temperature, oxygen vacancies are formed in LSM.

The cathodic reaction can simultaneously occur via all three paths, and for each path, one or more elementary steps determine the corresponding reaction rate. Which elementary reaction will be rate-limiting step is not always predictable and may depend on local conditions like temperature and oxygen partial pressure or on microstructural conditions. In addition, there may be parallel reaction pathways and a crossover of these various reaction pathways may cause interference. For example, the incorporation rate into the cathode (bulk path) depends on the surface concentration of adsorbed oxygen and thus can be influenced by the surface diffusion occurring via the electrode surface path mechanism. Despite the complicated nature of the reaction mechanism, oxygen reduction mechanistic studies provide very insightful understanding information, especially on well-defined systems [20]. The use of dense thin films [21, 22] and microelectrodes [23, 24] with well-defined geometry has provided insights into the kinetics of ORR by quantitative correlation of cathode geometry with ORR impedance.

Reducing the operating temperature of SOFCs has advantages for many practical applications. However, a decrease in temperature is concurrent with an increase in polarization losses. This phenomena is typified by the example shown in Fig. 3 [25]. When the temperature was decreased, the cathodic overpotentials of two cathode materials markedly increased. Thus, the key technical challenge is how to minimize electrode polarization losses especially at the cathode/electrolyte interface at lower operating temperatures.

The electrode polarization losses are usually associated with the generation and transport of oxygen ions within the porous cathode structure [26]. The Adler or ALS model [27] could provide a strategy for optimizing the composition and structure of electrodes to obtain good performance at intermediate temperatures. Providing that values for the oxygen self-diffusion coefficient (D^*, $cm^2\ s^{-1}$), oxygen surface exchange coefficient (k, $cm\ s^{-1}$), and appropriate microstructural parameters are available, the heterogeneous chemical reaction contribution (R_{chem}) can be calculated by the ALS model as shown in Eq. 2.

$$R_{chem} = \frac{RT}{2F^2}\sqrt{\frac{\tau}{(1-\varepsilon)aC_0^2D^*k}} \tag{2}$$

where τ, ε, and a are tortuosity, fractional porosity, and internal surface area/unit volume, respectively, C_0 is the surface concentration of oxygen.

Isotopic exchange is an important technique to determine the oxygen diffusion in mixed ionic-electronic conducting materials [28, 29]. For example, Kilner et al. [29] measured the oxygen surface exchange and oxygen tracer diffusion coefficients of $La_{0.8}Sr_{0.2}MnO_{3+\delta}$ using the

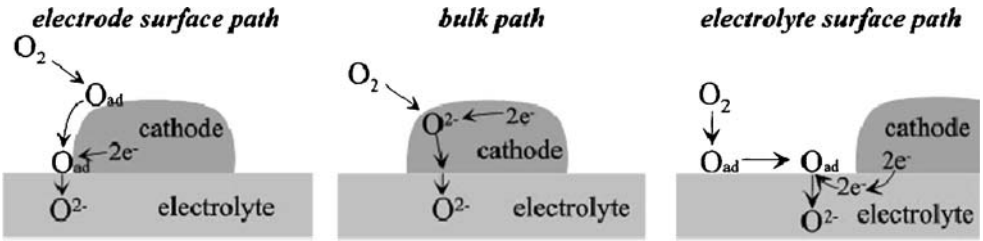

Fig. 2 Sketches of the three reaction paths of the oxygen reduction and incorporation reaction and some possible rate-determining steps. Modifications of the paths (e.g., adsorption of a molecular rather than an atomic species or diffusion along the cathode/electrolyte interface) and a combination of electrode and electrolyte surface paths (adsorption on cathode and surface diffusion onto the electrolyte surface) are also possible [20]. Copyright © 2003 Annual Reviews

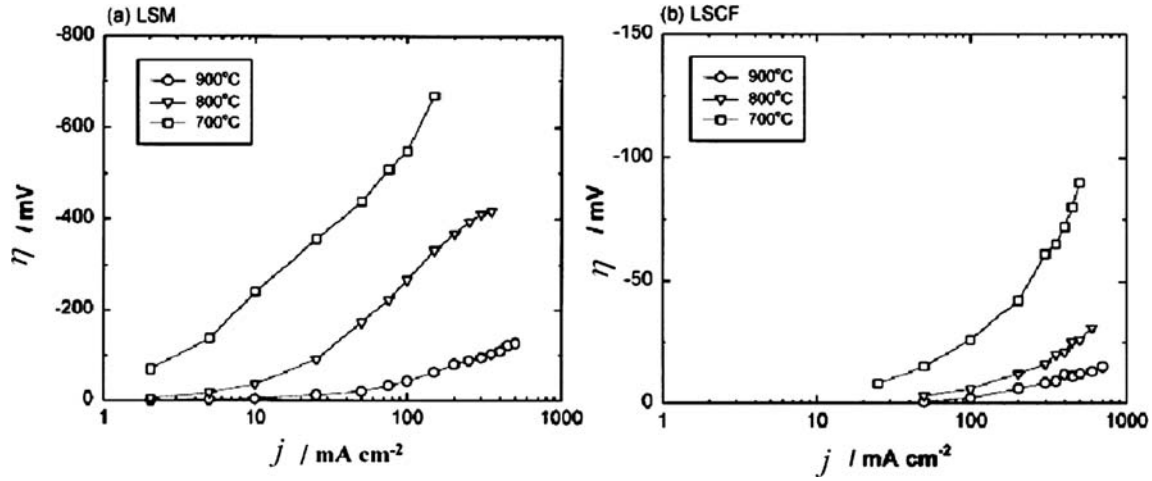

Fig. 3 Steady-state polarization curves of LSM and LSCF electrodes measured at different temperatures in air [25]. Copyright © 2002 Elsevier B.V.

$^{18}O/^{16}O$ isotope exchange depth profile method, obtaining $k = 1.0 \times 10^{-8} cms^{-1}$ and $D^* = 3.2 \times 10^{-13} cm^2 s^{-1}$ at 900°C.

Usually, the polarization losses of the cathode can be decreased by two approaches. On one hand, it can be achieved by choosing an appropriate composition to improve the kinetics of oxygen exchange and diffusion [30] bearing in mind that the TEC of cathodes should be matched with those of other components. On the other hand, it can also be achieved by optimizing the microstructure at the cathode/electrolyte interface to extend the TPB length. Endo et al. [31] studied the electrochemical properties of three microstructural types (dense, porous, and porous/dense double layer) of cathode materials based on $La_{1-x}Sr_xCoO_3$ (LSC) and $La_{1-x}Sr_xMnO_3$ (LSM). Their results revealed that surface area is an important factor for reaction rate on the LSC electrode and high performance electrodes can be obtained by using a mixed ionic and electronic conducting electrode with a large surface area. For the MIEC cathodes, the role of surface area in improving their performance lies in the fact that a higher surface area leads to more active sites for the oxygen reduction reaction because the electrochemical reactions can only occur at the TPBs.

An alternative method to enhance cathode activity is utilizing cathodic biasing or polarization [32–34], which has been shown to significantly reduce the oxygen reduction reaction overpotential on porous LSM [35, 36] and LSM-YSZ composites [37, 38]. This phenomenon is called the activation effect [39] or hysteretic behavior of cathodes [40]. It not only influences the surface microstructural and compositional changes of the cathode but also causes a morphological change at the interface between the cathode and electrolyte under the polarization/biasing treatment. The ORR activity was enhanced via oxygen vacancy formation associated with surface and compositional changes adjacent to TPBs [33] or by promoting direct incorporation of oxygen from the gas into the electrolyte due to partially reduced manganese oxide [32]. However, until now, there is no general consensus about the mechanism responsible for electrode activation or for the hysteretic behavior.

In recent years, new in situ experimental technologies are leading to new insight into the cathode reaction mechanism. Conventional electrochemical techniques such as impedance spectroscopy and voltammetry can provide detailed information about the rates of processes occurring in situ. However, these techniques are not informative for directly assigning which molecular species participate in the electrochemical reactions. In contrast, optical spectroscopy is capable of identifying the molecular structures present on the SOFC electrode surfaces. Lu et al. [41] developed a potential dependent Fourier Transform Infrared Spectroscopy technique (pd-FTIRES) to obtain information on oxygen species adsorbed directly onto the functioning cathode surface as a function of temperature, overpotential, and oxygen partial pressure. Although they believed that evidence for two or possibly three distinct dioxygen species present on the electrode surface were found, the separation of bulk phonon modes from surface species is usually difficult. Horita et al. [42] observed by secondary-ion mass spectrometry imaging technique that the active sites for oxygen reduction on the O_2/LSM/YSZ were spots around the triple-phase boundaries. The width of the active sites for oxygen reduction was estimated to be less than 1 μm under the examined conditions.

Quantum chemical calculations could also play a vital role in rational design of better electrode materials for SOFCs. Wang et al. [43] studied the interactions between oxygen molecules and a silver surface or a $CeO_2(111)$-supported atomic layer of silver using first-principle calculations. Their results showed that the O_2 dissociation process on a monolayer of silver supported by $CeO_2(111)$

(TPB) with oxygen vacancies has a lower reaction barrier than on silver surfaces (two-phase boundary), and the dissociated oxygen ions can quickly bond with subsurface cerium atoms via a highly exothermic reaction with no barrier. The computed energies of the reactions show the O_2 reduction process, and the incorporation of the dissociated O^{2-} ions in the oxide electrolyte prefer to take place at the TPB region with oxygen vacancies, consistent with experimental observations, suggesting that the rate of oxygen reduction may be enhanced by increasing the TPB areas. Recently, Choi et al. [44] studied the catalytic mechanism of oxygen reduction on $La_{0.5}Sr_{0.5}MnO_3$ (110) surfaces in solid oxide fuel cells using density functional theory (DFT) and molecular dynamics calculations. Their results suggest that O_2 species are preferentially adsorbed on the Mn site rather than the La site according to the difference in adsorption energy, which supports the fact that B-site cations are more active than A-site cations for oxygen reduction on several perovskite-type ABO_3 cathode materials. The atomic and molecular oxygen adsorption and diffusion on $LaMnO_3$ (001) surfaces were also studied by Kotomin et al. [45] using ab initio DFT plane–wave supercell calculations. They concluded that the dissociative adsorption of O_2 molecules from the gas phase is energetically favorable on the surface Mn ions even on a defect-free surface. The adsorbed O atoms could penetrate the electrode plane first when much more mobile surface oxygen vacancies approach the O ions strongly bound to the surface Mn ions. Direct incorporation of the O_2 molecule into an O vacancy is also energetically favorable.

Development of cathode materials

Physical properties of perovskite cathode materials

Perovskite materials have been widely used as cathode materials in SOFCs [46]. In order to better design and optimize the cathode materials, it is necessary to first understand the fundamentals of the perovskite structure. A perovskite-type oxide has the general formula ABO_3, in which A and B are cations with a total charge of +6. The lower valence A cations (such as, La, Sr, Ca, and Pb, etc.) are larger and coordinated to twelve oxygen anions while the B cations (such as, Ti, Cr, Ni, Fe, Co, and Zr, etc.) occupy the much smaller space and are coordinated to six oxygen anions. Full or partial substitution of A or B cations with cations of different valence is possible. When the overall valence of the A-site and B-site cations (n + m) adds up to less than six, the missing charge is made up by introducing vacancies at the oxygen lattice sites [47, 48]. Figure 4 shows the typical structure of the cubic perovskite ABO_3 [47].

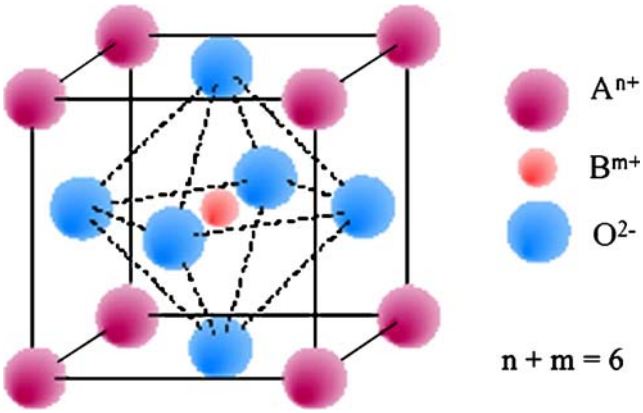

Fig. 4 Unit cell of the ABO_3 perovskite structure [47]. Copyright © 2003 Nature Publishing Group

Many perovskite structures are distorted and do not have cubic symmetry. Common distortions such as cation displacements within the octahedra and tilting of the octahedra are related to the properties of the A and B substituted atoms. The degree of distortion in ABO_3 perovskites can be determined according to the Goldschmidt tolerance factor (t) as follows:

$$t = (r_A + r_B)/\sqrt{2}(r_B + r_O) \quad (3)$$

where r_A, r_B, and r_O are the effective ionic radii of A, B, and O ions, respectively. Usually, this factor is evaluated from Shannon's ionic radii [49] for respective coordination numbers. When the tolerance factor is near unity, the structure is the ideal cubic one. Smaller A or bigger B cations give rise to a decrease in tolerance factor with a cation displacement and tilting of corner sharing BO_6 octahedra to an orthorhombic symmetry [50].

For most of the perovskite materials used as cathodes in SOFCs, the A-site cation is a mixture of rare and alkaline earths (such as La and Sr, Ca or Ba), while the B-site cation is a reducible transition metal such as Mn, Fe, Co, or Ni (or a mixture thereof). Therefore, in most cases, a redox catalytic mechanism is usually provided by B-site cations [51]. The octahedral symmetry around the transition metal often promotes a metallic or semiconducting band structure at high temperatures leading to high electronic conduction. With a rational choice of A- and B-site cations, a large and stable number of oxygen ion vacancies can be introduced at SOFC operating conditions, thus facilitating significant bulk ionic oxygen transport [12].

For $A_{1-x}A'_xBO_3$ perovskite-type oxides resulting in substoichiometric oxygen-to-metal regions, an oxygen vacancy scenario results [52, 53], e.g., in $Ln_{1-x}^{3+}Sr_x^{2+}M^{3+}O_{3-\delta}$, the oxygen vacancies arise either from substitution of A^{3+} by A^{2+} or from the partial reduction of B^{3+} or B^{4+} to B^{2+} and B^{3+}, respectively. Oxygen mobility through vacancies is the basis of oxide ion conductivity. In some compositions of perovskite-

type oxides, the oxide ion conductivities are as high as those observed in solid electrolyte materials, e.g., the ionic conductivity of $Sr_{0.9}Ce_{0.1}CoO_{3-\delta}$ reaches 0.133 S cm^{-1} at 800 °C in air [54–56]. In general, most cathode materials rely on doping of both the A- and B-sites to improve electrical conductivity and electrocatalytic performance.

Besides the electrical and structural characteristics mentioned above, thermodynamic data are essential for evaluating and predicting the long-term stability of perovskite cathode materials and their compatibility with other components at SOFC operating temperatures. The thermodynamic stability of perovskite cathode materials was discussed in terms of the stabilization energies and the valence stabilities by Yokokawa et al. [57, 58]. By determining the enthalpies of formation for the perovskite $LaMnO_3$ (M = Cr, Fe, Co, and Ni) at room temperature using high-temperature oxide melt solution calorimetry, Navrotsky et al. [59] concluded that the relative thermodynamic stability of the perovskite $LaMnO_3$ decreases in the order of Cr, Fe, Co, Ni. Tanasescu et al. correlated the thermodynamic properties with the compositional variables of perovskite ABO_3 (A = La, Sr; B = Mn, Fe, Co) by a coulometric titration technique coupled with EMF measurements [60–62]. The thermodynamic properties were represented by the relative partial molar free energies, enthalpies, and entropies of oxygen dissolution in the perovskite phase.

Lanthanum manganite-based cathodes

LSM cathode

Oxygen nonstoichiometry and oxygen defects have a great effect on the ionic and electronic transport properties of cathode materials. $LaMnO_3$-based oxides have either oxygen-excess or oxygen-deficient nonstoichiometry. This is generally formulated by $La_{1-x}A_xMnO_{3\pm\delta}$ (A is divalent cation, such as Sr^{2+} or Ca^{2+}; "+" denotes oxygen excess, and "–" denotes oxygen deficiency). Mizusaki et al. [53, 63, 64], Anderson [65, 66], and Nowotny et al. [67] studied in detail the oxygen nonstoichiometry of $La_{1-x}Sr_xMnO_{3\pm\delta}$ as a function of oxygen partial pressure, temperature, and composition. Various defect models have been proposed to explain the defect structure of the doped $LaMnO_3$ oxides.

For lanthanum manganite, the most commonly used dopant is strontium because its size matches with lanthanum. The Sr dopant in $La_{1-x}Sr_xMnO_{3\pm\delta}(x \leq 0.5)$ does not increase the oxygen vacancy concentration, a common phenomenon in most of the other perovskite cathode materials studied but rather oxidizes the manganese ion according to Eq. 4 [68, 69].

$$Mn_{Mn}^{\times} + SrO \xleftrightarrow{LaMnO_3} Sr_{La}^{'} + Mn_{Mn}^{\cdot} + O_O^{\times} \quad (4)$$

This reaction effectively increases the electron-hole concentration and improves the electrical conductivity. The electronic conductivity of LSM increases approximately linearly with increasing Sr concentration up to a maximum around 50 mol% [69]. At high temperature, $LaMnO_3$ undergoes a solid-phase reaction with YSZ to form $La_2Zr_2O_7$ (LZ) at the electrode–electrolyte interface [35, 70–72]. A little amount of Sr substitution decreases the reactivity of LSM compound with YSZ. However, $SrZrO_3$ (SZ) forms when Sr concentration is above about 30 mol% [72–75]. Therefore, an Sr content of 30 mol% is considered as optimal against the formation of unwanted electronically insulating phases. Incorporating a slight A-site deficiency in the materials can further decrease unwanted reactivity.

The relative amounts of LZ and SZ depend on the La/Sr ratio in the LSM [73, 76] and increase with increasing reaction time and sintering temperature [73, 77, 78]. The conductivity of these zirconates is two to three orders of magnitude lower than that of YSZ and therefore must strictly be avoided in order to prevent high ohmic loss. In addition, it was found that nonstoichiometry at the La site in $LaMnO_3$ plays an important role in the reaction [79]. Diffusion of Mn into YSZ leads to increases in La activity at the interface and promotes the interfacial reaction.

Mitterdorfer et al. [80] studied in detail nucleation and growth of LZ between porous $La_{0.85}Sr_{0.15}Mn_yO_{3+\delta}$ with (001) oriented 9.5 mol% doped YSZ single crystals using many characterization approaches. The insulating LZ phase between LSM and YSZ will interfere with two possible processes, which induce undesired polarization. One is surface diffusion of electroactive oxygen along the LSM surface to the TPBs; the other is the electrochemical formation of O^{2-} at the TPB due to limited availability of electronic charge carriers.

Other manganite cathodes

Generally, the electrical properties of manganite-based perovskite compounds are not sufficient for operation at temperatures below 800 °C. The absence of oxygen vacancies in LSM restricts the reduction of oxygen to the three-phase boundary regions. This limitation is the primary reason why LSM does not have acceptable performance at lower temperatures. Usually, two approaches have been taken to improve the performance of LSM cathodes so that they may be used at lower temperatures [68]. The first is to add a second ionically conducting phase to LSM. As mentioned above, this extends the surface area over which the oxygen reduction can occur. The second approach has been to replace La with other rare earth elements or dope LSM with a cation (such as, Co, Fe, or Ni) that promotes the formation of oxygen vacancies when strontium is doped on the A-site. In this subsection, the latter is mainly discussed.

The cathodic overpotentials of manganite cathodes can be modified greatly by replacing different rare-earth cations at the A site [81, 82]. Ishihara et al. [81] systematically studied the cathodic overpotentials of $Ln_{0.6}Sr_{0.4}MnO_3$ (Ln = La, Pr, Nd, Sm, Gd, Yb, or Y). The Sr-doped $PrMnO_3$ cathode showed low overpotential values even at decreased operating temperatures. Sr-doped $PrMnO_3$ also exhibits a compatible thermal expansion coefficient with YSZ. Consequently, they concluded that doped $PrMnO_3$ is a promising cathode material for IT-SOFCs. In addition, the formation of undesired pyrochlore phases $Ln_2Zr_2O_7$ between LSM cathode and YSZ electrolyte can be suppressed for those having smaller lanthanoids especially the $Pr_{1-x}Sr_xMnO_3$, $Nd_{1-x}Sr_xMnO_3$, and $Sm_{1-x}Sr_xMnO_3$ systems [83].

More Sr substitution and an increase of the atomic number of lanthanides are beneficial to adjust the TEC of $Ln_{1-x}Sr_xMnO_3$ to match with those of the electrolytes. Kostogloudis et al. [84] found that $Nd_{1-x}Sr_xMnO_{3\pm x}$ $(x = 0.4, 0.5)$ with a TEC of 12.3×10^{-6} K^{-1} demonstrated thermal and chemical compatibility with GDC electrolytes. $Pr_{0.5}Sr_{0.5}MnO_3$ showed high electrical conductivity of 226 S cm^{-1} at 500 °C [85], which is expected to increase with temperature indicating a potentially promising cathode material for SOFCs.

The majority of work performed on the lanthanide manganite materials has concentrated on the cases where the A site is Sr-doped. In terms of chemical compatibility and electrical conductivity, however, Ca-doped ones have proven more promising. $Pr_{0.7}Ca_{0.3}MnO_3$ showed chemical stability and was thermally compatible (11.9×10^{-6} K^{-1}) with YSZ electrolyte materials [86]. Its conductivity is close to that of the previously mentioned Sr-doped PrMnO3 with the same composition.

As for the doping at the B-site, Sc-doped manganite $La_{0.8}Sr_{0.2}Mn_{1-x}Sc_xO_{3-\delta}$(LSMS) is a potential cathode material for IT-SOFCs [87]. Nonstoichiometric defects are introduced into the perovskite lattice of LSMS samples by Sc substitution, which leads to an increased oxygen ion mobility in the samples containing Sc. However, high-level doping of Sc (>10 mol%) results in the segregation of Sc_2O_3 secondary phases at elevated temperatures. The cells with LSMS cathodes exhibit higher performance, especially at lower temperatures, which can be ascribed to the increased oxygen vacancies in the LSMS. For this cathode material, the high cost of scandium may be a concern for applications.

$Sr_{1-x}Ce_xMnO_{3-\delta}$ system are also potential cathode materials for IT-SOFCs. The TECs of $Sr_{1-x}Ce_xMnO_{3-\delta}$ $(0.1 \le x \le 0.3)$ varies between 12.4×10^{-6} and 10.1×10^{-6} K^{-1}, close to that of CeO_2-based electrolytes [88]. By doping Co in the B-site, the area-specific resistance of $Sr_{0.8}Ce_{0.2}Mn_{0.8}Co_{0.2}O_{3-\delta}$ is 0.10 Ω cm^2 at 750 °C, which is about 20 times lower than that of $Sr_{0.8}Ce_{0.2}MnO_{3-\delta}$ [89]. The $Sr_{0.8}Ce_{0.2}Mn_{0.8}Co_{0.2}O_{3-\delta}$ cathode shows high catalytic activity for oxygen reduction in the temperature range of 700–800 °C.

Lanthanum cobaltite and ferrite cathodes

Cobaltite cathodes

$LaCoO_3$ exhibits a rather high electronic density of states near the Fermi level (E_F) [90]. The marked catalytic properties of $LaCoO_3$ are associated with electron occupation of the crystal field d state near E_F and with the buildup of surface charge so as to enhance the electron transfer between a surface cation and a potentially catalyzed species.

$La_{1-x}Sr_xCoO_{3-\delta}$ exhibits a complex behavior with regard to the dependence of nonstoichiometry, electrical, and magnetic properties on the strontium content, temperature, and oxygen partial pressure. It is of interest to consider the defect structure of these oxides. Petrov et al. [91] proposed a defect model associated with the defect structure of $La_{1-x}Sr_xCoO_{3-\delta}$ in which strontium ions are assumed to occupy the regular La lattice sites, Sr_{La}', leading to predominantly electron holes. In order to maintain electrical neutrality, the substitution of Sr ions must be compensated by the formation of equivalent positive charges, comprising $Co_{Co}^{\cdot}$ and oxygen vacancies $\left[V_O^{\cdot\cdot}\right]$. The overall electroneutrality condition is then given by

$$Sr_{Sr}^{\times} + Co_{Co}^{\cdot} + 2V_O^{\cdot\cdot} = Sr_{La}' + Co_{Co}^{\times}, \tag{5}$$

$$2Co_{Co}^{\cdot} + O_O^{\times} \rightarrow 2Co_{Co}^{\times} + V_O^{\cdot\cdot} + \frac{1}{2}O_2(g), \tag{6}$$

and

$$\left[V_O^{\cdot\cdot}\right]\left[Co_{Co}^{\times}\right]^2 = K_{V_O^{\cdot\cdot}}\left[Co_{Co}^{\cdot}\right]^2\left[O_O^{\times}\right]P_{O_2}^{-1/2}, \tag{7}$$

where $Co_{Co}^{\cdot}$ and $Co_{Co}^{\times}$ denote Co^{4+} and Co^{3+} ions at a normal Co site, respectively, and $K_{V_O^{\cdot\cdot}}$ is the equilibrium constant.

Usually, cobalt-based materials display higher ionic and electronic conductivities than other cathode materials. Therefore, the use of cobalt-containing cathode materials should result in a decreased cathode polarization resistance. $La_{1-x}Sr_xCoO_{3-\delta}$ has a marked electrode activity due to high oxygen diffusivity and high dissociation ability of oxygen molecules [92]. However, a large amount of cobalt results in an increased thermal expansion coefficient, which may result in a delamination at the cathode/electrolyte interface or cracking of the electrolyte [93]. By substituting the La cation with an alternative cation, such as Gd or Pr, a decrease in the ASR and TEC can be expected to occur. The TECs of $Ln_{0.6}Sr_{0.4}CoO_{3-\delta}$(Ln = La, Pr, Nd, Sm, and Gd) decrease from La to Gd. A similar trend has also been

observed in the analogous $Ln_{1-x}Sr_xMnO_3$ and $Ln_{0.8}Sr_{0.2}Fe_{0.8}Co_{0.2}O_3$ systems [93, 94]. The large TEC of the cobaltites ($\sim 20\times10^{-6}$ K^{-1}) compared with that of the manganites ($\sim 11\times10^{-6}$ K^{-1}) is due to the formation of oxygen vacancies, spin-state transitions associated with Co^{3+} [95], and the relatively weaker Co–O bond compared with the Mn–O bond [96].

Doping Cu into the Co site can further enhance the ionic conductivity and catalytic activity of $(La,Sr)CoO_{3-\delta}$, although the electrical conductivity of $(La,Sr)(Co,Cu)O_{3-\delta}$(LSCC) was lower [97]. Among perovskites with different rare earth cations at the A-site, those incorporating Pr^{3+} exhibited the highest electrical conductivity and the lowest overpotential values due to the additional contribution of Pr^{3+}/Pr^{4+} valence change [98]. A combination of Pr, Sr for the A-site, and Co, Cu for the B-site material $Pr_{1-x}Sr_xCo_{1-y}Cu_yO_{3-\delta}$ was studied by Zhu et al. [99]. Their results indicated that $Pr_{0.7}Sr_{0.3}Co_{1-y}Cu_yO_{3-\delta}$ materials $(y = 0.05 - 0.3)$ had lower overpotential compared with those of $Pr_{0.7}Sr_{0.3}CoO_{3-\delta}$ and especially low overpotentials for compounds with the $Pr_{0.7}Sr_{0.3}Co_{0.9}Cu_{0.1}O_{3-\delta}$ composition. The maximum power density of an anode-supported cell consisting of $Pr_{0.7}Sr_{0.3}Co_{0.9}Cu_{0.1}O_{3-\delta}$ cathode, SDC electrolyte, and NiO/$Ce_{0.8}Sm_{0.2}O_{1.9}$ anode reached 481 mW cm^{-2} at 750°C.

For Mn doping at the B-site, Chen et al. [100] observed that $La_{0.6}Sr_{0.4}Co_{0.8}Mn_{0.2}O_{3-\delta}$ has the lowest cathodic overpotential among the tested $Ln_{0.6}Sr_{0.4}Co_{0.8}Mn_{0.2}O_{3-\delta}$ $(Ln = La, Gd, Sm, orNd)$ compounds at 500–800 °C. The electrical conductivity of $La_{0.6}Sr_{0.4}Co_{0.8}Mn_{0.2}O_{3-\delta}$ reaches about 1,400 S cm^{-1} at 500 °C. However, these oxides also have large thermal expansion coefficients greater than 18×10^{-6} K^{-1}.

Sr-doped samarium cobaltite ($Sm_{1-x}Sr_xCoO_3$, SSC) is another widely studied cathode material for IT-SOFCs showing a higher electrical conductivity. The electrical conductivity increases with Sr doping and a maximum conductivity is usually observed at x=0.5. The electrical conductivity of this composition shows metallic-like behavior and reaches up to 10^3 S cm^{-1} in the temperature range of 800–1100 °C [101, 102]. Although SSC has been studied as a cathode material for SOFCs with yttria-stabilized zirconia [103], $La_{1-x}Sr_xGa_{1-y}Mg_yO_3$ [102] and doped ceria electrolyte [104], its thermal expansion coefficient is greater than 20×10^{-6} K^{-1}, which could produce stresses at the interface during thermal cycling. In addition, reactivity tests of $Sm_{1-x}Sr_xCoO_3$ with YSZ show that $Sm_{1-x}Sr_xCoO_3$ is stable below 800 °C because $SrZrO_3$ is formed only above 900 °C [103].

Besides the disadvantage of high thermal expansion coefficient, cobaltite cathodes react readily with YSZ to form insulating compounds during the sintering process, which degrades their performance. Therefore, a diffusion barrier layer is necessary for the cells consisting of cobaltite-based cathodes and the YSZ electrolyte [105, 106].

Ferrite cathodes

Lanthanum ferrite ($LaFeO_3$) is expected to be more stable than cobaltite perovskites because the Fe^{3+} ion has a stable electronic configuration $3d^5$. Sr-doped $LaFeO_3$ (LSF) cathodes have shown promising performance with respect to the power density and stability at 750 °C [107–109]. In iron-based cathodes, reactivity with YSZ electrolyte is significantly reduced. In addition, TECs of the ferrite–perovskite are relatively close to those of the YSZ and CGO electrolyte.

The addition of Sr to $LaFeO_3$ creates Sr_{La}', thus causing a charge unbalance. The charge neutrality is then maintained by the formation of Fe^{4+} ions or oxygen vacancies ($V_{\ddot{o}}$). The highest theoretical conductivity expected by Sr addition would be at x=0.5 creating a maximum Fe^{4+}/Fe^{3+} ratio of 1:1 [110]. At high temperatures, LSF will lose oxygen to form oxygen vacancies at the cost of decreasing hole concentration. This reaction can be represented in Kröger-Vink notation:

$$2Fe_{Fe}^{\cdot} + O_O^{\times} \rightarrow \frac{1}{2}O_2 + 2Fe_{Fe}^{\times} + V_O^{\cdot\cdot} \quad (8)$$

where $Fe_{Fe}^{\cdot}$ represents Fe ions in the 4+ valence state (similar to holes), $Fe_{Fe}^{\times}$ denotes Fe cations in 3+ valence state, and $V_{\ddot{o}}$ represents the oxygen vacancy. Under relatively high oxygen partial pressures (e.g., air or O_2), holes are the predominant charge carriers while at lower oxygen partial pressures Sr_{La}' defects are compensated by oxygen vacancies [111]. Because of the much higher mobility of the electrons or holes than that of oxygen ions, the total conductivity in ferrites is dominated by holes rather than oxygen ions. Therefore, the total conductivity in ferrites is dominated by a hole-conduction mechanism [110].

By incorporating La deficiency in $La_{0.8}Sr_{0.2}FeO_3$, Ralph et al. [107] found that the ASR of this cathode was significantly reduced and reached 0.1 Ω cm^2 at 800 °C. The thermal expansion coefficient of the $La_{0.7}Sr_{0.25}FeO_3$ cathode closely matches with those of CGO and YSZ. This cathode has demonstrated no degradation over a 500-h operation indicating a promising material for lower-temperature SOFCs.

Simner et al. [108] found that an anode-supported cell consisting of $La_{0.8}Sr_{0.2}FeO_3$ cathode, YSZ electrolyte, and NiO–YSZ anode exhibited a powder density as high as about 0.9–0.95 W cm^{-2} at 750 °C and 0.7 V and exhibited excellent stability over a 300-h test period. In addition, they found that Sr-doped $LaFeO_3$ showed significant variability in performance depending on the type of current collectors used [112]. The use of platinum and silver current collectors is accompanied by the improved cell performance and stability while the cell utilizing gold cathode current collectors

shows a severe degradation of performance. Similar effects caused by different current collectors on other cathode materials have not yet been reported.

Cu-doped lanthanum strontium ferrite showed superior kinetics for the electrochemical reduction of oxygen [113]. The current densities of cells with $La_{0.7}Sr_{0.3}Cu_{0.2}Fe_{0.8}O_3$ as a cathode are approximately two to three times higher than that with $La_{0.7}Sr_{0.3}FeO_3$ and ten times higher than that with $La_{0.8}Sr_{0.2}FeO_3$ as a cathode. Copper doping significantly reduces the allowable sintering temperatures during the electrode fabrication. An enhanced low-temperature sintering of a Sr-doped lanthanum ferrite composition $(La_{0.8}Sr_{0.2})_{0.98}Fe_{0.98}Cu_{0.02}O_3$ (with 2-mol% Cu-doping and 2-mol% A-site deficiency) has also been observed below 1,000 °C by Simmer et al. [114]. The cathode can be sintered onto YSZ without significant Zr^{4+} diffusion into the perovskite. However, the Cu-doped composition does exhibit chemical interaction with YSZ (typically above 950 °C), resulting in the precipitation of monoclinic zirconia. Initial single-cell studies utilizing a $(La_{0.8}Sr_{0.2})_{0.98}Fe_{0.98}Cu_{0.02}O_3$ cathode on an anode-supported YSZ cell have indicated power densities in the range of 1.35~1.75 W cm^{-2} at 750 °C and 0.7 V [113].

Although pure LSF is thermodynamically more stable than that of cobalt-containing perovskites [115], it was observed that its electrochemical performance was inferior to LSCF with a similar A-site stoichiometry [115–117]. A potential degradation mechanism for LSF cathodes is the interdiffusion of Zr and La [112, 118–120]. Anderson et al. [120] found that there are reactions of YSZ with $Ln_{0.8}Sr_{0.2}FeO_3 (Ln = La, Sr, Pr, or Nd)$ and $La_{0.8}Ba_{0.2}FeO_3$ with the sole exception being $La_{0.8}Ca_{0.2}FeO_3$ (LCF). The reactivity either results in secondary phase formation or incorporation of Zr into the perovskite B-site. For the case of Ca, it may be a consequence of a lower limit of Zr dissolution into the LCF compound due to its smaller unit cell volume. Therefore, protective ceria-based barrier layers are usually used to prevent the reaction between LSF and YSZ during the sintering step of cathodes [109, 120–122].

Ferro-cobaltite cathodes

$La_{1-x}Sr_xFe_{1-y}Co_yO_3$ shows good electrical conductivity, a high oxygen surface exchange coefficient, and a good oxygen self-diffusion coefficient between 600 and 800 °C. The oxygen self-diffusion coefficient of LSCF is 2.6×10^{-9} cm^2 s^{-1} at 500 °C, which is superior in performance to that of $La_{0.8}Sr_{0.2}MnO_3$ which has a oxygen self-diffusion coefficient of 10^{-12} cm^2 s^{-1} at 1,000 °C [123, 124]. In addition, LSCF does not react with ceria-based electrolytes [125, 126]. Although the electrical conductivity was found to decrease slightly as the Sr content decreased, the TECs were found to be the lowest for the composition with the highest A-site deficiency, that is $13.8\times 10^{-6}K^{-1}$ for $La_{0.6}Sr_{0.2}Co_{0.2}Fe_{0.8}O_{3-\delta}$ at 700°C. This TEC value matches commonly used electrolytes [127].

Usually, the increase of ionic conductivities is more influenced by Sr concentration at the A-site while the increase of the electronic conductivities is more influenced by Fe and Co concentration at the B-site. The A-site deficiency has only a small effect on the TEC while a higher Sr content results in a higher TEC due to higher oxygen vacancy concentrations. Mai et al. [117] recently observed that a small A-site deficiency and a high strontium content had a particularly positive effect on the cell performance using $La_{1-x-y}Sr_xCo_{0.2}Fe_{0.8}O_{3-\delta}$ as a cathode material. The measured current densities of cells consisting of $La_{1-x-y}Sr_xCo_{0.2}Fe_{0.8}O_{3-\delta}$ cathode, CGO electrolyte, and a NiO–YSZ anode were as high as 1.76 A cm^{-2} at 800 °C and 0.7 V, which is about twice the current density of cells with LSM/YSZ cathodes.

At lower operation temperatures, LSCF-based cathodes are superior to LSM-type cathodes due to a lower area-specific resistance. However, LSCF-type perovskites are generally incompatible with YSZ electrolytes due to undesirable interface reactions. Therefore, a CGO diffusion barrier layer is used to prevent the formation of low conductive compounds without negatively affecting the electrochemical performance [128, 129]. Another cause of higher degradation rates for cells with LSCF cathodes lies in the diffusion of strontium out of LSCF, which leads to a strontium depletion in the cathode and significantly lower performance. It has been observed that the cells with slightly less Sr in the cathode$(La_{0.58}Sr_{0.38}Co_{0.2}Fe_{0.8}O_{3-\delta})$ showed lower performance than that of the $La_{0.58}Sr_{0.4}Co_{0.2}Fe_{0.8}O_{3-\delta}$ [130, 131]. It has been found that partial decomposition of the perovskite usually has greater influence on the cell degradation than interface reactions during the operation [132, 133].

Although the magnitudes of the electrical conductivity and thermal expansion of the $La_{0.8}Sr_{0.2}(Mn, Fe, Co)O_{3-\delta}$ perovskite are mainly dependent on the percentage of Co in the compositions [134], substitution of the La cation at A-sites by Pr cation with multiple valence states can further improve the cathode performance. Meng et al. [135] investigated $Pr_{1-x}Sr_xCo_{0.8}Fe_{0.2}O_{3-\delta}(PSCF)(x = 0.2 \sim 0.6)$ as cathode materials for IT-SOFCs. Their results showed that the material with a composition of $Pr_{0.6}Sr_{0.4}Co_{0.8}Fe_{0.2}O_{3-\delta}$ has the highest conductivity, 1,040 S cm^{-1}, at 300 °C. The ASR of the PSCF–GDC (50:50 by weight) cathode is as low as 0.046 Ω cm^2 at 800 °C. The power densities of the electrolyte-supported cell consisting of PSCF-GDC cathodes, a GDC electrolyte, and a NiO–GDC anode reach 520 mW cm^{-2} at 800 °C and 303 mWcm^{-2} at 700 °C. All these results indicate that PSCF-GDC (50:50 by weight) is a promising cathode material for IT-SOFCs. Colomer et al.

[30] studied the $Sr_{0.8}Ce_{0.1}Fe_{0.7}Co_{0.3}O_{3-\delta}$(SCFC) cathode material for IT-SOFCs. The area-specific resistivity of SCFC electrodes is 0.86 Ω cm^2 at 700 °C. They suggested that the enhanced oxygen ion diffusion in SCFC provides superior cathodic performances compared with that of LSCF at 700 °C.

$Ba_{0.5}Sr_{0.5}Co_{0.8}Fe_{0.2}O_{3-\delta}$(BSCF) has been studied as an excellent oxygen permeation membrane material in the last decade. Haile and Shao [136] first employed BSCF as a cathode material in a solid oxide fuel cell using hydrogen as the fuel. They found that the peak power densities of an anode-supported cell consisting of a NiO-SDC anode, an SDC electrolyte, and a BSCF cathode reach 1,010 and 402 mW cm^{-2} at 600 °C and 500 °C, respectively. The area-specific resistances of this material are 0.055–0.071 and 0.51–0.61 Ω cm^2 at 600 and 500 °C, respectively, which are considerably lower than that of other perovskite type cathode materials under similar operation conditions. Although this potential cathode material shows excellent electrochemical performance, the obvious disadvantage of BSCF is the high TEC, with a value of 20×10^{-6} K^{-1} between 50 °C and 1,000 °C [137], as is common with Co-containing perovskites. This indicates that thermal cycling could be problematic for cells using this cathode material due to a mismatched TEC with those of other cell components. In order to solve the issue of thermal expansion, one possibility is to make composite cathode materials with BSCF. However, the introduction of the composite may lessen the BSCF performance.

For most of the perovskite oxides containing alkaline-earth elements, one stability concern is that they could react with gas species such as CO_2, SO_2, or water vapor, especially with carbon dioxide from the air, at a significant rate at temperatures less than 800 °C [138–143]. Since the presence of CO_2 and water vapor is a characteristic of atmospheric air, these materials for SOFCs are preferably operated at temperatures above 800 °C. Otherwise, a prepurification process for air is required to remove carbon dioxide when using strontium cobaltite- or strontium manganite-based cathodes at temperatures below 800 °C [144].

Yan et al. [145] investigated the effect of CO_2 on the performance of a BSCF cathode. They found that the BSCF cathode is susceptible to CO_2 even in relatively small quantities at temperature ranges of 450–750 °C and especially at lower temperatures. The poisoning effect of CO_2 on the performance of BSCF is further aggravated when the CO_2 content increases and the temperature decreases. The deterioration of BSCF performance by carbon dioxide is reversible up to 550 °C. A further decrease of the operation temperature irreversibly reduced the single cell performance. It was found that the presence of CO_2 inhibits the oxygen reduction process over the BSCF cathode surface and consequently decreases the cell performance. In the case of single chamber systems fed with hydrocarbons, a high concentration CO_2 is produced. Therefore, the BSCF cathode is not suitable for single chamber fuel cells using hydrocarbons as fuels especially at low temperatures.

Nickelate cathodes

At atmospheric oxygen pressure, perovskite type nickelate $LaNiO_{3-\delta}$ is stable only below 1230–1270 K; further heating leads to decomposition into $La_2NiO_{4+\delta}$ with a K_2NiF_4-type structure and NiO, via the separation of Ruddlesden–Popper (RP) type $La_4Ni_3O_{10-\delta}$ and$La_3Ni_2O_{7-\delta}$ phases at intermediate stages [146–148]. These transformations limit the practical use of $LaNiO_{3-\delta}$-based materials, and they can be partly suppressed by a doping into the nickel sublattice [147].

Iron-doped nickelate $LaFe_{1-x}Ni_xO_{3-\delta}$ exhibits an attractive combination of electronic transport properties, a moderate thermal expansion, and phase stability in air. Researchers at NTT Corporation in Japan have been investigating $LaNi_{0.6}Fe_{0.4}O_3$ (LNF) as a cathode material for SOFCs operated at intermediate temperatures [148–150]. LNF has many desirable characteristics, including a high electrical conductivity, less mismatch of thermal expansion coefficient with a zirconia electrolyte, high catalytic activity, and high durability against the cathode poisoning by volatile chromium species from metallic components [151, 152]. The electronic conductivity of LNF is 580 S cm^{-1} at 800 °C [148]. The average thermal expansion coefficient of LNF is lower (11.4×10^{-6} K^{-1}) than that of $La_{0.8}Sr_{0.2}MnO_3$ $\left(12.0\times10^{-6}K^{-1}\right)$ and closer to the TEC value of 8YSZ (10.5×10^{-6} K^{-1}). Unfortunately, LNF is more reactive toward ZrO_2-based electrolytes than conventional La(Sr)MnO_3 at temperatures used for sintering [150]. The amount of $La_2Zr_2O_7$ formation rapidly increases when the sintering temperature of the LNF cathode exceeded 1,000 °C. A preloading treatment at a very high current density (>1.0 A cm^{-2}) causes current-voltage characteristics of cells using LNF as the cathode to be improved significantly. An anode-supported cell consisting of 10 mol % Sc_2O_3-1 mol% Al_2O_3-stabilized ZrO_2 (SASZ) electrolyte, a NiO–SASZ anode, and an LNF cathode sintered at 1,000 °C exhibited a maximum power density of 1.56 W cm^{-2} at 800 °C.

Recently, an improvement of the initial performance of the LNF cathode was observed by placing an active layer consisting of $Ce_{0.8}Sm_{0.2}O_{1.9}$ (SDC) or $Ce_{0.9}Gd_{0.1}O_{1.95}$ (GDC) and LNF particles between the LNF cathode and a scandia alumina-doped zirconia electrolyte [153]. It was found that the LNF tends to react with SDC when the sintering temperature is 1,100 °C or higher. However, this reaction does not seem to affect the performance of LNF

cathodes containing a LNF–SDC active layer when the sintering temperature is below 1,250 °C.

For the Sr-doped LNF (LSNF), the electronic conductivity reached a peak value when the total concentration of Ni and Sr is about 0.6 in the temperature range of 600–800 °C [149]. The conductivity of LSNF exhibits temperature dependence similar to that of metals when the concentrations of Ni and Sr are high. However, the conductivities drop sharply when the temperature exceeds about 600 °C, which is probably caused by an increase in the oxygen vacancy concentration, rather than by the degradation of the structure symmetry. An oxygen vacancy increase is expected to decrease the electronic conduction of perovskite oxides.

As a reference for choice of cathode materials in SOFC systems, Table 2 summarizes the thermal expansion coefficients and electronic and ionic conductivities of a number of perovskite-type cathode materials.

K_2NiF_4 type structure cathode materials

$La_2NiO_{4+\delta}$-based compounds have a K_2NiF_4-type structure and are usually formulated as $A_2BO_{4+\delta}$, which is described as a stacking of perovskite ABO_3 layers alternating with rock salt AO layers along the c-direction [164] as shown in Fig. 5 [165]. Such oxides are of interest as an oxygen electrode material for applications in various solid electrolyte devices. This is primarily associated with the high electronic conductivity of $A_2BO_{4+\delta}(B = Co, Ni, Cu)$ compounds and solid solutions based on them due to the mixed valence of the B-site metal. In addition, a high concentration of oxygen interstitials offers the possibility of rapid oxygen transport through the ceramic material and thus provides a new type of mixed ionic electronic conductor cathode materials.

Taking $La_{2-x}Sr_xCoO_{4+\delta}$ oxides as an example, the following defect model was proposed for K_2NiF_4-type structure oxides by Vashook et al. [166]. In the $La_{2-x}Sr_xCoO_{4+\delta}$ oxide, $Sr_{La}^{'}$ and $V_O^{\cdot\cdot}$ are assumed to exist as defects. The reaction can be represented in Kröger-Vink notation:

$$2SrO + 2La_{La}^{\times} + O_O^{\times} \Leftrightarrow 2Sr_{La}^{'} + La_2O_3 + V_O^{\cdot\cdot} \quad (9)$$

Co^{3+} cations can disproportionate into $Co^{2+}\left(Co_{Co}^{'}\right)$ and $Co^{4+}\left(Co_{Co}^{\cdot}\right)$. An increase of conductivity of $Sr-$doped $LaCoO_{4+\delta}$ with oxygen partial pressure could be understood as the result of an increasing concentration of holes according to the following reaction

$$2Co_{Co}^{\times} + 0.5O_2 + V_O^{\cdot\cdot} \Leftrightarrow 2Co_{Co}^{\cdot} + O_O^{\times} \quad (10)$$

The electrical conductivities of the $A_2BO_{4+\delta}$-type nickelates and cobaltites are of a p-type conduction mechanism. These compounds reach nearly 100 S cm^{-1} at 800 °C under high oxygen partial pressures. At lower oxygen partial pressures, their conductivities decrease slower than that of some perovskite oxides [167].

The oxygen diffusivity of $La_{2-x}Sr_xNiO_{4+\delta}$ is higher than that of LSCF, particularly at lower temperatures, but lower than that of LSC [168]. In addition, $La_{2-x}Sr_xNiO_{4+\delta}$ appears to be more stable than either of these two materials in terms of thermal behavior at high temperatures. The thermal expansion coefficient of $La_2NiO_{4+\delta}$ is$13.7 \times 10^{-6}K^{-1}$, which matches well with those of possible electrolyte materials such as YSZ or CGO. Recently, Zhao et al. [169] found that the interfacial polarization resistance of $La_{1.2}Sr_{0.8}Co_{0.8}Ni_{0.2}O_{4+\delta}$-based electrodes was 1.36 Ω cm^2 at 600 °C when the electrode was not activated. Current treatment performed at 200 mA cm^{-2} caused an activation increase within 30 min. The power density of an anode-supported single cell consisting of a $La_{1.2}Sr_{0.8}Co_{0.8}Ni_{0.2}O_{4+\delta}-$GDCcathode, a GDC electrolyte, and a NiO–GDC anode reached 350 mW cm^{-2} at 600 °C. This composite cathode shows potential application in SOFCs, although the long term-stability remains unproven.

Doping at the La-site with alkaline-earths (Sr, Ba, Ca) and other rare earths (Nd or Pr), or doping at the Ni-site with other transition metals (typically Cu or Co) may lead to dramatic changes of the structural and physical properties. $La_2Ni_{1-x}Cu_xO_{4+\delta}(0 \le x \le 1)$ has been evaluated as a possible cathode material for SOFCs [170]. The thermal expansion coefficients are in the range of $10.8 \sim 13.0 \times 10^{-6}K^{-1}$. Lower ASR values are obtained with a LSGM electrolyte compared with those with 8YSZ as an electrolyte material. For the $La_2Ni_{0.6}Cu_{0.4}O_{4+\delta}$ composition, the total conductivity reached 87 S cm^{-1} at 580 °C.

The $Ba_{1.2}Sr_{0.8}CoO_{4+\delta}$- GDC (70:30 by weight) composite cathode showed a low polarization, 0.17 Ω cm^2, on a GDC electrolyte [171]. However, similar to that of $Ba_{0.5}Sr_{0.5}Co_{0.8}Fe_{0.2}O_3$, this material may also be susceptible to reactions with CO_2 in air.

Effect of addition of noble metal phases

As the operating temperature is reduced, electrode polarization losses increase. The cathode thus becomes the limiting component for further progress. One way to overcome this limitation may be adding a certain amount of noble metal, such as, palladium, silver, or platinum to the cathode. The addition of noble metal phases to an active cathode layer is mainly used to enhance the oxygen reduction reaction.

The melting point of silver is 961 °C. Metallic silver is a potential component for the cathode in SOFCs operated at less than 800 °C because of its good catalytic activity, high electrical conductivity, and its relatively low cost. A composite cathode consisting of high ionic conductivity

Table 2 Perovskite-type oxide materials: thermal expansion coefficient (*TEC*), electronic (σ_e), and ionic conductivities (σ_i) in air

Composition	TEC ($\times 10^{-6} K^{-1}$)	T (°C)	σ_e (Scm^{-1})	σ_i (Scm^{-1})	References
$La_{0.8}Sr_{0.2}MnO_3$	11.8	900	300	5.93×10^{-7}	[25]
$La_{0.7}Sr_{0.3}MnO_3$	11.7	800	240	–	[70, 154]
$La_{0.6}Sr_{0.4}MnO_3$	13	800	130	–	[71, 98]
$Pr_{0.6}Sr_{0.4}MnO_3$	12	950	220	–	[98]
$La_{0.8}Sr_{0.2}CoO_3$	19.1	800	1,220	_	[134, 155]
$La_{0.6}Sr_{0.4}CoO_3$	20.5	800	1,600	0.22	[56, 156]
$La_{0.8}Sr_{0.2}FeO_3$	12.2	750	155	–	[108, 134]
$La_{0.5}Sr_{0.5}FeO_3$	–	550	352	–	[111]
	–	800	369	0.205	[157]
$La_{0.6}Sr_{0.4}FeO_3$	16.3	800	129	5.6×10^{-3}	[56, 158]
$Pr_{0.5}Sr_{0.5}FeO_3$	13.2	550	300	–	[159]
$Pr_{0.8}Sr_{0.2}FeO_3$	12.1	800	78	–	[159]
$La_{0.7}Sr_{0.3}Fe_{0.8}Ni_{0.2}O_3$	13.7	750	290	–	[108]
$La_{0.8}Sr_{0.2}Co_{0.8}Fe_{0.2}O_3$	20.1	600	1,050	–	[159]
$La_{0.8}Sr_{0.2}Co_{0.2}Fe_{0.8}O_3$	15.4	600	125	–	[160]
$La_{0.6}Sr_{0.4}Co_{0.8}Mn_{0.2}O_3$	18.1	500	1,400	–	[100]
$La_{0.6}Sr_{0.4}Co_{0.8}Fe_{0.2}O_3$	21.4	800	269	0.058	[161, 162]
$La_{0.6}Sr_{0.4}Co_{0.2}Fe_{0.8}O_3$	15.3	600	330	8×10^{-3}	[56, 163]
$La_{0.4}Sr_{0.6}Co_{0.2}Fe_{0.8}O_3$	16.8	600	–	–	[163]
$La_{0.8}Sr_{0.2}Co_{0.2}Fe_{0.8}O_3$	14.8	800	87	2.2×10^{-3}	[56]
$La_{0.8}Sr_{0.2}Co_{0.8}Fe_{0.2}O_3$	19.3	800	1,000	4×10^{-2}	[56, 161]
$La_{0.6}Sr_{0.4}Co_{0.9}Cu_{0.1}O_3$	19.2	700	1,400	–	[97]
$Pr_{0.8}Sr_{0.2}Co_{0.2}Fe_{0.8}O_3$	12.8	800	76	1.5×10^{-3}	[56]
$Pr_{0.7}Sr_{0.3}Co_{0.2}Mn_{0.8}O_3$	11.1	800	200	4.4×10^{-5}	[56]
$Pr_{0.6}Sr_{0.4}Co_{0.8}Fe_{0.2}O_3$	19.69	550	950	–	[135]
$Pr_{0.4}Sr_{0.6}Co_{0.8}Fe_{0.2}O_3$	21.33	550	600	–	[135]
$Pr_{0.7}Sr_{0.3}Co_{0.9}Cu_{0.1}O_3$	–	700	1236	–	[99]
$Ba_{0.5}Sr_{0.5}Co_{0.8}Fe_{0.2}O_3$	20	500	30	–	[137]
$Sm_{0.5}Sr_{0.5}CoO_3$	20.5	700~900	>1,000	–	[102, 104]
$LaNi_{0.6}Fe_{0.4}O_3$	11.4	800	580	–	[148]
$Sr_{0.9}Ce_{0.1}Fe_{0.8}Ni_{0.2}O_3$	18.9	800	87	0.04	[56]

copper-subtituted bismuth vanadates ($Bi_2V_{0.9}Cu_{0.1}O_{5.35}$) and silver was used for low-temperature SOFCs by Xia et al. [172]. This composite cathode exhibits a remarkable catalytic activity for oxygen reduction at 500–550 °C and greatly reduces the cathode–electrolyte interfacial polarization resistances down to about 0.53 Ω cm^2 at 500 °C. The power density of an anode-supported cell consisting of a NiO–GDC anode, a GDC electrolyte, and a Ag-$Bi_2V_{0.9}Cu_{0.1}O_{5.35}$ composite cathode reaches 0.231 W cm^{-2} at 500 °C.

Different methods have been used to prepare Ag-based composite cathode. Wang et al. [173] reported that the Ag coating improved the oxygen exchange reaction activity of $L_{0.6}Sr_{0.4}Co_{0.8}Fe_{0.2}O_3 - CGO - Ag$ composite cathode and interface conductivities at 600 °C. Ag nanoparticle-infiltration is another effective and low-cost approach to improve the cathode performance [174, 175]. Recently, Sakito et al. [175] observed that the infiltration of ~18 wt.% Ag fine particles into LSCF results in ~50% enhancement of power density. The Ni–GDC/GDC/LSCF–Ag cell shows a maximum power density of 0.415 W cm^{-2} at 530 °C, which is very attractive for IT-SOFCs. Ag was also co-sputtered with LSC by a dc magnetron sputtering method [176]. The interfacial resistance of $La_{0.7}Co_{0.3}O_3 - (Y_2O_3)_{0.25}(Bi_2O_3)_{0.75}$ decreases from 0.4 Ω cm^2 at 750 °C to 0.3 Ω cm^2 by the addition of 30 vol.% Ag. The Ag–LSC electrodes showed good stability during 200 h annealing at 750 °C. Although silver-based cathodes show good electrochemical properties, it should be pointed out here that oxygen is easily dissolved into silver and forms an Ag/Ag_2O solid solution. In addition, even far below its melting point, silver is relatively mobile. Therefore, these concerns should be addressed prior to a long-term application of silver-based cathodes in SOFCs.

Pd is another noble metal widely used to improve the cathode performance in SOFCs. Sahibzada et al. [177] investigated the effect of the addition of Pd to a LSCF

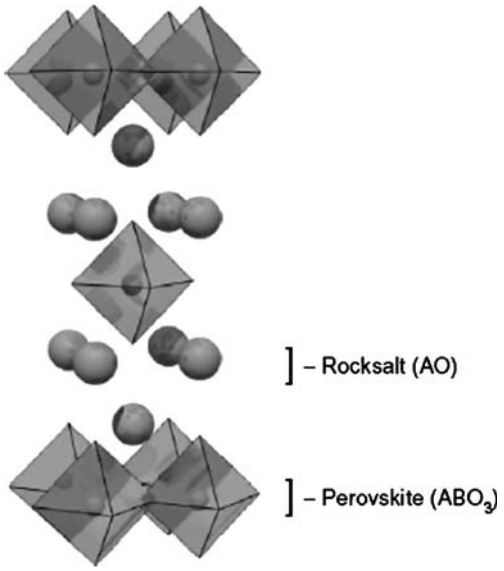

Fig. 5 K_2NiF_4 type structure showing alternating AO and ABO_3 layers [165]. Copyright © 2005 Elsevier B.V.

cathode and found the overall cell resistances decreased by 15.5% at 650 °C and 40% at 550 °C indicating a promotion effect of Pd. Simmer et al. [109] also observed that Pd-facilitated initial performance improvements in the $La_{0.8}Sr_{0.2}FeO_{3-\delta} - Ce_{0.8}Sm_{0.2}O_{1.9}$ cathode with respect to the catalytic activity for O_2 reduction. However, this enhancement is not sustainable and is followed by a rapid degradation of power density in less than 24 h compared with reference cells fabricated without Pd additions. The alloying of Pd particles with Pt that has presumably migrated from the cathode current collector may be responsible for the observed degradation phenomenon, which is confirmed by SEM/EDX examinations. This is also indirectly confirmed by Haanappel's results [178] that the addition of Pt to cathode materials does not positively affect the electrochemical performance of cells. Haanappel et al. [178] systematically studied the effects of Pd prepared by different methods on the catalytic activity of cathodes for the oxygen reduction. They found that neither infiltration of the cathode with Pd solution nor mixing with Pd black results in a positive effect. The catalytic effect was only observed with Pd loading on activated carbon. The well-dispersed Pd particles on an activated carbon support may be the reason for the increased catalytic effect. This also explains why their results are different from Simmer's work [109]. Usually, the particle size, the distribution, and the crystallinity of noble metals in the cathode play an important role on their catalytic activity. Therefore, a similar composition of materials prepared by different methods may show different results. As for the application of Pd on activated carbon, the stability and lifetime under SOFC operating conditions are potential concerns. It should be pointed out here that the addition of noble metals, in particular Pt, does not seem a good solution to improve the performances of cells since one target to commercialization of SOFC is to decrease price.

Microstructure optimization of cathode materials

The length of the three-phase boundary correlates well with the interfacial resistances to electrochemical oxidation of fuels at the anode [179–181] and reduction of oxygen at the cathode [31, 182–185]. Therefore, an extension of the TPB and an increase of the number of active reaction sites become necessary to improve electrode performances. This can be achieved by developing electrode materials with a higher mixed ionic-electronic conductivity and optimizing the microstructure of electrodes.

Nanostructured electrode materials with significantly higher surface areas have demonstrated superior electrochemical properties [186]. Liu et al. [183] reported the fabrication of nanostructured and functionally graded composite cathodes, which are graded in microstructure as well as in composition, using a combustion CVD process. Their results showed that nanostructured electrodes dramatically reduce the cathode/electrolyte interfacial polarization resistances (0.17 Ω cm^2). The power density of an anode-supported cell consisting of a SSC–SDC cathode, a GDC electrolyte, and a Ni–SDC anode reached 0.375 W cm^{-2} at 600 °C while the long-term stability of these electrodes was not reported.

In recent years, the wet impregnation method has showed promise in the development of nanostructured electrodes with high performance. Many examples can be found in two recent review papers [40, 187]. Huang et al. [188] found that adding LSCo to an LSM-YSZ cathode by the infiltration method had a dramatic effect on performance but forming a mixed Sr-doped $LaCo_{0.2}Mn_{0.8}O_3$ did not. Mixed conductivity at the three-phase boundary may explain the improved performance. The impregnation of nanoscale particles, forming connected networks, into solid oxide fuel cell electrodes has also been shown to lead to considerable improvement in performance [189]. Impedance analysis of the impregnated electrode suggests that the particular microstructure of the nanoparticulate pore-wall coating minimizes the rate-limiting step in the oxygen reduction reaction within LSM-YSZ cathodes.

Although the wet impregnation method has demonstrated to be an effective technique to achieve advantageous microstructures and a high performance, the durability of these materials is a big concern over long periods at high temperatures. Generally, the nanosized particles tend to aggregate at a high temperature, and the catalytic activity decreases with the operation time.

In addition, it should be noted that materials synthesized by different methods usually have very different microstructures and properties. For cathode materials with the same composition, the materials prepared by a sol–gel or glycine–nitrate combustion method usually have much smaller grain size and higher surface area compared with those prepared by a conventional solid-phase reaction, thus leading to better cell performances. However, the feasibility of scale-up and cost of these processes must be taken into account when considering incorporation into practical applications.

Chromium-resistant cathode materials for IT-SOFCs

In recent years, IT-SOFCs have received much attention as potential power generation systems with the potential for high efficiency operation. An obvious advantage of IT-SOFCs is that metallic alloys can be used as interconnect materials, which significantly reduces the system cost. In particular, chromium-containing ferritic stainless steels are the most promising and widely used oxidation-resistant alloys due to their appropriate thermal expansion behaviors and low cost. However, the application of chromium-containing alloys still poses many challenges even at reduced temperatures. For instance, the oxide scale formed on the surface of the alloys after a long exposure in the SOFC environment results in a high electrical resistance that eventually degrades cell performance [190, 191]. In addition, under high temperatures and oxidizing atmospheres, volatile chromium (Cr) species such as CrO_3 and $CrO_2(OH)_2$ are generated [192, 193]. These species can cause rapid performance deterioration in SOFCs due to the poisoning of cathodes such as (La,Sr)MnO_3 and (La,Sr) (Co,Fe)O_3 toward the oxygen reduction reaction [194–199]. The poisoning is largely due to the deposition of Cr species at the electrode/electrolyte interface regions or on the electrolyte surface.

Figure 6 shows the influence of steel samples with and without coatings on the performance of anode-supported single cells consisting of a YSZ electrolyte, a Ni/YSZ cermet anode, and a (La,Sr) (Co,Fe)O_3 cathode, operated at 700–800 °C with a hydrogen fuel [200, 201]. Without the presence of the steel sample, no degradation was observed. Introduction of the Crofer22 steel coupon into the chamber of the tested cell resulted in a rapid degradation of cell voltage although the current flow was not passed through the steel. Samples treated with a protective $(Cr,Mn)_3O_4$ spinel layer on the surface of Crofer22 did not show this effect, even when examined over a nearly 2,000-h operation. Further tests are needed to confirm this behavior over a time period ranging from 3,000 to 8,000 h. Preliminary evaluation of chromium content in the cathode material shows a distinct correlation with the amount of chromium present in the air supplied to the cathode.

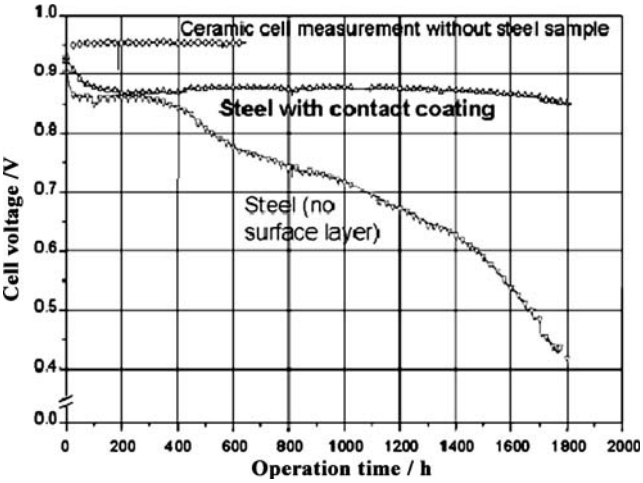

Fig. 6 Influence of steel samples with and without coating on the performance of single cells [200]. Copyright © 2006 Wiley-Blackwell

Possible mechanism of chromium deposition at cathodes

Taniguchi et al. [202, 203] made extensive investigations on chromium poisoning of lanthanum strontium manganite in terms of the overpotential of cathodes, thermodynamic activity of Cr_2O_3, and water vapor content in the cathode compartment. These observations provide a fundamental understanding of the degradation mechanisms presented in cathode reactions.

The vapor pressure of chromium-containing species over Cr_2O_3 or other chromium-containing oxides has been thoroughly investigated and is summarized as follows [187, 204]:

(1) Effect of oxygen partial pressure: CrO_3(g), CrO_2(g), and CrO(g) have different vapor pressures over Cr_2O_3 and vary as a function of the oxygen potential. With increasing oxygen partial pressure, the equilibrium vapor pressure of each species increases. Under dry air, CrO_3 is the predominately present species.
(2) Effect of water vapor: Since $CrO_2(OH)_2$(g) and other species containing O and H are relatively stable, the H_2O vapor pressure is also an important factor. Under humid air, the predominant volatile species is $CrO_2(OH)_2$.
(3) Effect of temperature: The vapor pressure of CrO_3(g) exhibits large temperature dependence, while the vapor pressure of $CrO_2(OH)_2$(g) is small.

Yokokawa et al. [205] considered chromium poisoning from the viewpoint of thermodynamic stability of the perovskite cathodes. The Cr_2O_3 deposition or spinel $CrMn_2O_4$ formation on the TPBs is a direct cause of chromium poisoning.

The interaction between alloy interconnects and cathodes in SOFCs have been extensively investigated. In the earlier

studies, Badwal et al. [195] and Taniguchi et al. [202] considered that the deposition of Cr species is closely related to the oxygen activity at the electrode/electrolyte interface. The deposition of Cr species is believed mainly by the electrochemical reduction of gaseous Cr species to solid Cr_2O_3 in competition with the oxygen reduction reaction. However, Konysheva et al. [194] recently reported that the degradation of cells by chromium poisoning could have two causes. On one hand, the Cr species may react with some cathode materials to form poorly conductive phases, such as $SrCrO_4$; on the other hand, the deposited solid chromium oxide species may block the gaseous oxygen diffusion and transportation as well as the active TPBs. In recent years, Jiang et al. [206–210] proposed that the Cr deposition process at the SOFC cathode is, in principle, a non-electrochemical process. The deposition process is kinetically limited by nucleation reactions between the gaseous Cr species and nucleation agents. The reactions can be generally written as follows [210, 211]:

$$1/2Cr_2O_3(\text{oxide scale}) + 3/4O_{2(g)} \rightarrow CrO_{3(g)} \quad (11)$$

$$CrO_3 + N \rightarrow Cr - N - O_x(\text{nuclei}) + O_2 \quad (12)$$

$$Cr - N - O_x(\text{nuclei}) + CrO_3 \rightarrow Cr_2O_3 \quad (13)$$

where N denotes the nucleation agent. Similarly, Cr deposition steps can also be written for other gaseous Cr species. In the case of the LSM electrode, the nucleation agent has been identified to be the manganese species (i.e., Mn^{2+}) generated under cathodic polarization conditions [207, 208] and for the LSCF electrode, it is the SrO species enriched originally or segregated at the electrode surface [197, 206]. Further reactions between the nuclei, gaseous Cr species, and nucleation agents lead to the deposition and formation of $(Cr,Mn)_3O_4$ and $SrCrO_4$ [206–209].

$$Cr - N - O_x(\text{nuclei}) + CrO_3 + Mn^{2+} \rightarrow (Cr,Mn)_3O_4 \quad (14)$$

$$Cr - N - O_x(\text{nuclei}) + CrO_3 + SrO \rightarrow SrCrO_4 \quad (15)$$

The mechanism of the Cr deposition process proposed above by Jiang et al. [212] seems more reasonable. It implies that cathode materials, which are free of nucleation agents (such as Mn- and Sr-containing species), would be more tolerant toward the Cr deposition.

Figure 7 schematically illustrates the possible poisoning mechanism of the cathode with chromium species. When $Cr_2O_{3(s)}$ is exposed to dry air at temperatures higher than approximately 873 K, CrO_3 vapor is easily produced from the surface of $Cr_2O_{3(s)}$. Furthermore, the presence of a little amount of water vapor in air significantly increases the vapor pressure of Cr species. The formation of the gaseous chromium oxide and oxyhydroxide species can be expressed as Eqs. 16, 17, 18, 19 [193]. The Cr content is also correlated with oxygen ion vacancy concentration in the cathode materials.

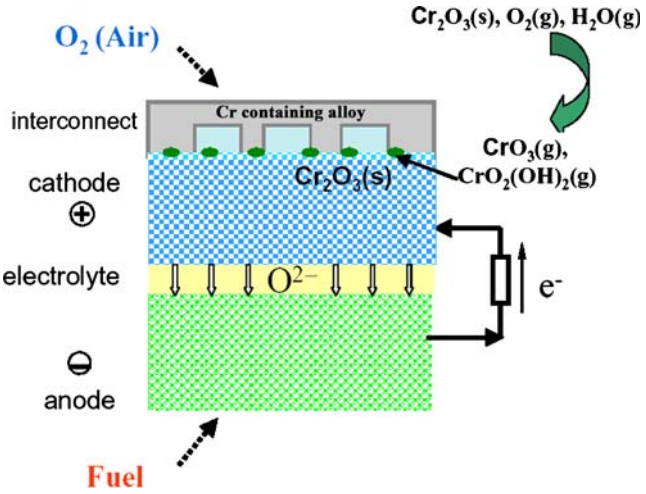

Fig. 7 Possible poisoning mechanism of the cathode with chromium species

$$2Cr + 1.5O_{2(s)} \rightarrow Cr_2O_{3(s)} \quad (16)$$

$$\frac{1}{2}Cr_2O_{3(s)} + \frac{3}{4}O_{2(g)} \rightarrow CrO_{3(g)} \quad (17)$$

$$Cr_2O_3 + O_{2(g)} + H_2O_{(g)} \rightarrow 2CrO_2(OH)_{2(g)} \quad (18)$$

$$2CrO_2(OH)_{2(g)} + 6e^- + 3V_{\ddot{o}} \rightarrow Cr_2O_3 + 3O_O^{\times} + 2H_2O \quad (19)$$

Development of chromium-resistant materials and processes for forming protective coatings

Zhen et al. [210] found that the Cr deposition processes at LSM and LSCF cathodes of SOFCs are kinetically limited by the nucleation reaction between gaseous Cr species and nucleation agents. In the case of the LSM electrode, it is SrO species segregated at the electrode surface. They also found that $LaNi_{0.6}Fe_{0.4}O_3$ and $La_{0.6}Ba_{0.4}Co_{0.2}Fe_{0.8}O_3$ electrodes are highly tolerant toward Cr deposition and are much more stable than LSM and LSCF cathodes under SOFC operation conditions in the presence of a Fe–Cr metallic interconnect.

Recently, Chen et al. [212] found that chromium deposition depends strongly on the Ba composition in $(La_{0.6}Sr_{0.4-x}Ba_x)(Co_{0.2}Fe_{0.8})O_3$ (LSBCF) $(0 \le x \le 0.4)$ cathode. For the case of LSCF (x=0), the Cr deposition is most significant,

completely covering the surface of the electrode after a polarization at 200 mA cm^{-2} for 1,200 min. As the Sr content in LSBCF decreases (i.e., Ba content increases), the Cr deposition was reduced significantly. $BaCrO_4$ is the main phase of the Cr deposit on the surface of the LSBCF when x reaches 0.4. The LSBCF electrodes show similar electrocatalytic activities toward the O_2 reduction reaction in the absence of Fe–Cr interconnects and at early stages in the presence of Fe–Cr interconnects. Their results clearly show that significant differences in the Cr deposition are closely related to the Sr and Ba content and are not related to the electrochemical activities of the LSBCF cathodes.

Komatsu et al. [213] investigated the chemical reactivity of $LaNi_{0.6}Fe_{0.4}O_3$ with Cr_2O_3 at 1,073 K. Their results indicated that LNF shows much better chemical stability against Cr poisoning. They also investigated the effect of Cr poisoning on various cells consisting of either $LaNi_{0.6}Fe_{0.4}O_3$ or $La_{0.8}Sr_{0.2}MnO_3$ as a cathode and either yttria-stabilized zirconia or alumina-doped scandia stabilized zirconia (SASZ) as an electrolyte [151]. They found that the cathodic overpotential was almost the same for cells with LNF cathodes, either in the presence or absence of Cr-containing alloy (Inconel 600). LSM cathodes in the presence of Inconel 600 exhibited a very steep increase in overpotential curves after applying a current. These results indicate that the LNF cathode is electrochemically stable for Cr poisoning compared with that of LSM cathodes. For Cr poisoning, the case of LSCF is similar to that of LSM [213], although LSCF is also a promising cathode material for IT-SOFCs especially when the metallic interconnects were coated with a protective barrier to prevent the volatilization of Cr species.

Chromium poisoning effects on $Sm_{1-x}Sr_xCoO_3$ and $Ba_{0.5}Sr_{0.5}Co_{0.8}Fe_{0.2}O_{3-\delta}$ have not been reported yet. Considering the results summarized above for LSM and LSCF, $SrCrO_4$ may also form on the surface of SSC and BSCF in the presence of a Cr source thus leading to a performance degradation of cells.

Kim et al. at PNNL [214] investigated the Cr poisoning effects of the Mn-containing ferritic stainless steel on the degradation behavior of various cathodes such as LSCF, LSF, and LNF. Their results show LSCF was the most reactive with Cr species, forming the $SrCrO_4$ phase throughout the entire cathode layer. In the case of LSF, Cr species blocked the "burn-in" behavior, of which the power density increased with time, possibly induced by Pt migration from cathode current collector to the cathode/YSZ interface. Pt was not detected in the cell tested with Crofer22, which showed a fade in power density with time. LNF, which does not contain Sr, revealed the least interaction with Cr among the tested cathodes. However, Cr species were still deposited around the cathode/electrolyte interface leading to Cr poisoning and degradation of cell performance.

It can thus be concluded from the results described previously that cathodes free of nucleation agents (Mn- and Sr-containing species), such as LNF, show the least interaction with Cr species and are the most tolerant toward Cr deposition among the tested cathodes. However, the chromium-poisoning issue cannot be solved only by development of new chromium-tolerant cathode materials. Therefore, protective coatings for metallic interconnectors, especially the spinel coatings of $(Co,Mn)_3O_4$ and $(Mn,Cr)_3O_4$, are also being explored in order to reduce the Cr volatilization. Spinel coatings may be an effective and feasible approach to solving chromium-poisoning issues during long-term operation. Chen et al. [215] at Lawrence Berkeley National Laboratory showed that Mn–Co-spinels are very promising coating materials with regard to the suppression of Cr_2O_3 subscale growth and serve to increase electronic conductivities of oxide scales. Kurokawa et al. [216] found $La_{0.65}Sr_{0.3}MnO_3$, $La_{0.6}Sr_{0.4}Co_{0.8}Fe_{0.2}O_3$, and $MnCo_2O_4$ coatings, prepared from submicron powders, decreased chromium volatility by a factor of 21–40 at 800 °C.

Various processes have also been used to deposit protective coatings on interconnect alloys in order to protect cathodes from chromium poisoning and improve metallic interconnect stability; Yang et al. [217] at Pacific Northwest National Laboratory fabricated manganese cobaltite spinel protection layers with a nominal composition of $Mn_{1.5}Co_{1.5}O_4$ on ferritic stainless steel by slurry coating technology. The results of thermal, electrical, and electrochemical investigations indicated that the spinel protection layers not only significantly decreased the contact resistance but also effectively acted as a barrier to both the oxygen inward and chromium outward diffusion. A long-term thermal cycling test demonstrated excellent structural and thermomechanical stability of these spinel protection layers. Other developed technologies for depositing various protective coatings on interconnect alloys include large area-filtered arc deposition (LAFAD) and hybrid-filtered arc-assisted electron beam physical vapor deposition (FA-EBPVD) technologies [218, 219] as well as pulsed DC magnetron sputtering technology [220]. Significantly improved thermal stability, low and stable ASR values, and a minimal Cr volatility were observed with coated alloy interconnects compared with the uncoated ones.

Summary and outlook

In summary, state of the art of cathode development in SOFCs has been reviewed in this paper with the main focus being the advantages and existing constraints of various cathode materials. In terms of the composition, oxygen nonstoichiometry and a presence of defects have a great effect on the ionic and electronic transport properties of cathode

materials. Sr-doping at the A-site or Sc-substitution at the B-site in perovskite materials enhances the ionic conductivity while Fe and/or Co doping on the B-site increases the electronic conductivity. However, Co doping also has great influence on the TEC of cathode materials. Alternatively, doping with a cation that contains multiple valence states, such as, Pr or Sm, tends to improve the electronic conductivity. Although the electrochemical performance of some alternative cathode materials is significantly higher than that of conventional LSM cathodes, problems persist in the areas of chemical stability and thermal expansion match with other cell components. Usually, a trade-off between electrochemical performance and thermal expansion may be necessary to identify an optimum cathode composition. In addition, a diffusion barrier layer is also necessary to prevent the elemental interdiffusion at electrolyte–cathode interfaces. In terms of the microstructure, TPBs have a great effect on the electrochemical performance of cathode materials, and it has been shown that the method of manufacture has a large impact on the final microstructure. Electrode materials with a porous structure stable at the necessary fabrication and operating conditions are desirable for improving the performance of SOFC cathodes. Furthermore, long-term stability is a significant factor to be considered for practical SOFC stack applications.

When chromium-containing alloys are used as components in IT-SOFCs, the migration of chromium via chromia scale volatilization into SOFC cathodes can lead to a severe degradation of cell performances. Among the well-studied cathode materials such as LSM, LSF, LSC, LSCF, LNF, SSC, and BSCF, it has been found that LNF, free of nucleation agents (e.g., Mn and Sr), is less reactive toward chromium species and has a better tolerance against poisoning than other cathode materials. LNF represents a promising cathode material for IT-SOFCs with resistance to chromium-poisoning. In addition, protective coatings for metallic interconnects are also an important step in order to reduce the Cr volatilization and prevent the oxidation of interconnector materials. Protective coatings may be an effective approach to solving the chromium-poisoning issue during long-term operation.

More fundamental studies on the reaction mechanisms and the kinetics of oxygen reduction in SFOC cathodes are highly desirable and the work should be intensified in the future. By means of in situ spectroscopy technology coupled with impedance spectroscopy measurements and the use of thin film or microelectrodes with well-defined geometry, it is possible to obtain new insights into the electrochemical oxygen reduction reaction mechanisms. This understanding will lead to the achievement of a rational design in new cathode materials and their microstructure. In addition, quantum chemical calculations may be an effective approach to elucidate the interactions between O_2 and the cathode since this technique can provide electronic structure, geometrical parameters, and energetics of bulk and adsorbed intermediate species. Improving the performance of the existing cathode materials can also be achieved through optimization of processing, composition, and microstructure. Work on the optimization of interfacial properties and stability is also necessary for stack development.

Acknowledgments The authors acknowledge the financial support from the National Research Council Canada-Institute for Fuel Cell Innovation. We would also like to thank the referees for their constructive comments and suggestions on an earlier version of the manuscript.

References

1. Sun CW, Stimming U (2007) J Power Sources 171:247
2. Singhal SC, Kendall K (2003) High temperature solid oxide fuel cells: fundamentals, design, and applications. Elsevier, Oxford, pp 1–22
3. Mogensen M, Kammer K (2003) Annu Rev Mater Res 33:321
4. Yamamoto O (2000) Electrochim Acta 45:2423
5. Yahiro H, Eguchi Y, Eguchi K, Arai H (1988) J Appl Electrochem 18:527
6. Mogensen M, Lindegaard T, Hansen UR, Mogensen G (1994) J Electrochem Soc 141:2122
7. Eguchi K, Setoguchi T, Inoue T, Arai H (1992) Solid State Ionics 52:165
8. Ishihara T, Matsuda H, Takita Y (1994) J Am Chem Soc 116:3801
9. Feng M, Goodenough JB (1994) Eur J Solid State Inorg Chem 31:663
10. Vasylechko L, Vashook V, Savytskii D, Senyshyn A, Niewa R, Knapp M, Ullmann H, Berkowski M, Matkovskii A, Bismayer U (2003) J Solid State Chem 172:396
11. Gorte RJ, Vohs JM (2003) J Catal 216:477
12. Alder SB (2004) Chem Rev 104:4791
13. Antoni L (2004) Mater Sci Forum 461–464:1073
14. Ivers-Tiffee E, Weber A, Schichlein H (2003) In: Vielstich W, Lamm A, Gasteiger HA (eds) Handbook of fuel cells, vol 2. Wiley, Chichester, p 587
15. Gellings PJ, Bouwmeester HJM (2000) Catal Today 58:1
16. Siebert E, Hammouche A, Kleitz M (1995) Electrochim Acta 40:1741
17. Jørgensen MJ, Mogensen M (2001) J Electrochem Soc 148:A433
18. Baumann FS, Fleig J, Habermeier HU, Maier J (2006) Solid State Ionics 177:1071
19. Serra JM, Vert VB, Betz M, Haanappel VAC, Meulenberg WA, Tiet F (2008) J Electrochem Soc 155:B207
20. Fleig J (2003) Annu Rev Mater Res 33:361
21. Endo A, Fukunaga H, Wen C, Yamada K (2000) Solid State Ionics 135:353
22. Ioroi TH, Uchimoto TY, Ogumi Z, Takehara Z (1998) J Electrochem Soc 145:1999
23. Brichzin V, Fleig J, Habermeier HU, Maier J (2002) Solid State Ionics 152–153:499
24. Koep E, Mebane DS, Das R, Compson C, Liu ML (2005) Electrochem Solid-State Lett 8:A592
25. Jiang SP (2002) Solid State Ionics 146:1
26. Adler SB, Lane JA, Steele BCH (1996) J Electrochem Soc 143:3554

27. Steele BCH, Hori KM, Uchino S (2000) Solid State Ionics 135:445
28. Burriel M, Garcia G, Santiso J, Kilner JA, Chater RJ, Skinner SJ (2008) J Mater Chem 18:416
29. De Souza RA, Kilner JA, Walker JF (2000) Mater Lett 43:43
30. Colomer MT, Steele BCH, Kilner JA (2002) Solid State Ionics 147:41
31. Endo A, Wada S, Wen CJ, Komiyama H, Yamada K (1998) J Electrochem Soc 145:L35–L37
32. Backhaus-Ricoult M, Adib K, St. Clair T, Luerssen B, Gregoratti L, Barinov A (2008) Solid State Ionics 179:891
33. La O' GJ, Savinell RF, Shao-Horn Y (2009) J Electrochem Soc 156:B771
34. Woo LY, Glass RS, Gorte RJ, Orme CA, Nelson AJ (2009) J Electrochem Soc 156:B602
35. Jiang SP, Love JG, Zhang JP, Hoang M, Ramprakash Y, Hughes AE, Badwal SPS (1999) Solid State Ionics 121:1
36. Wang W, Jiang SP (2006) Solid State Ionics 177:1361
37. McIntosh S, Adler SB, Vohs JM, Gorte RJ (2004) Electrochem Solid-State Lett 7:A111
38. Lee YK, Kim JY, Moon KI, HS PJW, Jacobson CP, Visco SJ (2003) J Power Sources 115:219
39. Jiang SP (2007) J Solid State Electrochem 11:93
40. Vohs JM, Gorte RJ (2009) Adv Mater 21:943
41. Lu X, Faguy PW, Liu ML (2002) J Electrochem Soc 149:A1293
42. Horita T, Yamaji K, Ishikawa M, Sakai N, Yokokawa H, Kawada T, Kato T (1998) J Electrochem Soc 145:3196
43. Wang JH, Liu ML, Lin MC (2006) Solid State Ionics 177:939
44. Choi YM, Lin MC, Liu ML (2007) Angew Chem Int Ed 46:7214
45. Kotomin EA, Mastrikov YA, Heifets E, Maier J (2008) Phys Chem Chem Phys 10:4644
46. Skinner SJ (2001) Int J Inorg Mater 3:113
47. Boukamp BA (2003) Nat Mater 2:294
48. Tao SW, Irvine JTS (2003) Nat Mater 2:320
49. Shannon RD (1976) Acta Cryst A 32:751
50. Nomura K, Tanase S (1997) Solid State Ionics 98:229
51. McEvoy AJ (2000) Solid State Ionics 135:331
52. Van RJAM, Cordfunke EHP (1991) J Solid State Chem 93:212
53. Mizusaki J (1992) Solid State Ionics 52:79
54. Trofimenko NE, Ullmann H (2000) J Eur Ceram Soc 20:1241
55. Ullmann H, Trofimenko N (1999) Solid State Ionics 119:1
56. Ullmann H, Trofimenko N, Tietz F, Stöver D, Ahmad-Khanlou A (2000) Solid State Ionics 138:79
57. Yokokawa H, Sakai N, Kawada T, Dokiya M (1992) Solid State Ionics 52:43
58. Yokokawa H, Kawada T, Dokiya M (1989) J Am Ceram Soc 72:152
59. Cheng J, Navrotsky A (2005) J Mater Res 20:191
60. Tanasescu S, Totir ND, Neiner D (2001) J Optoelectronics Adv Mater 3:101
61. Tanasescu S, Totir ND, Marchidan DI (1998) Electrochimi Acta 43:1675
62. Tanasescu S, Totir ND, Marchidan DI (1999) Solid State Ionics 119:311
63. Mizusaki J, Mori N, Takai H, Yonemura Y, Minamiue H, Tagawa H, Dokiya M, Inaba H, Naraya K, Sasamoto T, Hashimoto T (2000) Solid State Ionics 129:163
64. Miyoshi S, Hong J, Yashiro K, Kaimai A, Nigara Y, Kawamura K, Kawada T, Mizusaki J (2002) Solid State Ionics 154–155:257
65. Kuo JH, Anderson HU, Sparlin DM (1989) J Solid State Chem 83:52
66. Anderson HU (1992) Solid State Ionics 52:33
67. Nowotny J, Rekas M (1988) J Am Ceram Soc 81:67
68. Ralph JM, Schoeler AC, Krumpelt M (2001) J Mater Sci 36:1161
69. Minh NQ, Takahashi T (1995) Science and technology of ceramic fuel cells. Elsevier, Amsterdam
70. Yamamoto O, Takeda Y, Kanno R, Noda M (1987) Solid State Ionics 22:241
71. Kenjo T, Nishiya M (1992) Solid State Ionics 57:295
72. Clausen C, Bagger C, Bilde-Sørensen JB, Horsewell A (1994) Solid State Ionics 70–71:59
73. Stochniol G, Syskakis E, Naoumidis A (1995) J Amer Ceram Soc 78:929
74. Setoguchi T, Inoue T, Takebe H, Eguchi K, Morinaga K, Arai H (1990) Solid State Ionics 37:217
75. Yokokawa H, Sakai N, Kawada T, Dokiya M (1990) Solid State Ionics 40–41:398
76. van Roosmalen JAM, Corfdfunke EHP (1992) Solid State Ionics 52:303
77. Schäfer W, Koch A, Herold-Schmidt U, Stolten D (1996) Solid State Ionics 86–88:1235
78. Taimatsu H, Wada K, Kaneko H, Yamamura H (1992) J Am Ceram Soc 75:401
79. Kawada T, Sakai N, Yokokawa H, Dokiya M, Anzai I (1992) Solid State Ionics 50:189
80. Mitterdorfer A, Gauckler LJ (1998) Solid State Ionics 111:185
81. Ishihara T, Kudo T, Matsuda H, Takita Y (1994) J Am Ceram Soc 77:1682
82. Wen TL, Tu HY, Xu ZH, Yamamoto O (1999) Solid State Ionics 121:25
83. Sakaki Y, Takeda Y, Kato A, Imanishi N, Yamamoto O, Hattori M, Iio M, Esaki Y (1999) Solid State Ionics 118:187
84. Kostogloudis GCh, Ftikos Ch (1999) J Eur Ceram Soc 19:497
85. Kostogloudis GCh, Vasilakos N, Ftikos Ch (1997) J Eur Ceram Soc 17:1513
86. Rim HR, Jeung SK, Jung E, Lee JS (1998) Mater Chem Phys 52:54
87. Yue XL, Yan AY, Zhang M, Liu L, Dong YL, Cheng MJ (2008) J Power Sources 185:691
88. Hashimoto S, Iwahara H (1999) J Electroceram 4:225
89. Gu H, Chen H, Gao L, Zheng Y, Zhu X, Guo L (2008) Int J Hydrogen Energy 33:4681
90. Kojima I, Adachi H, Yasumori I (1983) Surf Sci 130:50
91. Petrov AN, Kononchuk OF, Andreev AV, Cherepanov VA, Kofstad P (1995) Solid State Ionics 80:189
92. Takeda Y, Kanno R, Noda M, Yamamoto O (1986) Bull Inst Chem Res 64:157
93. Weber A, Ivers-Tiffee E (2004) J Power Sources 127:273
94. Riza F, Ftikos Ch, Tietz F, Fischer WJ (2001) J Eur Ceram Soc 21:769
95. Huang K, Lee HY, Goodenough JB (1998) J Electrochem Soc 145:3220
96. Lee KT, Manthiram A (2006) J Electrochem Soc 153:A794
97. Yasumoto K, Inagaki Y, Shiono M, Dokiya M (2002) Solid State Ionics 148:545
98. Ishihara T, Kudo T, Matsuda H, Takita Y (1995) J Electrochem Soc 142:1519
99. Zhu CJ, Liu XM, Xu D, Yan DT, Wang DY, Su WH (2008) Solid State Ionics 179:1470
100. Chen WX, Wen TL, Nie HW, Zheng R (2003) Mater Res Bull 38:1319
101. Fukunaga H, Koyama M, Takahashi N, Wen C, Yamada K (2000) Solid State Ionics 132:279
102. Ishihara T, Honda M, Shibayama T, Minami H, Nishiguchi H, Takita V (1998) J Electrochem Soc 145:3177
103. Tu HY, Takeda Y, Imanishi N, Yamamoto O (1997) Solid State Ionics 100:283
104. Xia CR, Rauch W, Chen FL, Liu ML (2002) Solid State Ionics 149:11
105. Shiono M, Kobayashi K, Nguyen TL, Hosoda K, Kato T, Ota K, Dokiya M (2004) Solid State Ionics 170:1
106. Rossignol C, Ralph JM, Bae JM, Vaughey JT (2004) Solid State Ionics 175:59

107. Ralph JM, Rossignol C, Kumar R (2003) J Electrochem Soc 150:A1518
108. Simner SP, Bonnett JF, Canfield NL, Meinhardt KD, Sprenkle VL, Stevenson JW (2002) Electrochem Solid-state Lett 5:A173
109. Simner SP, Bonnett JF, Canfield NL, Meinhardt KD, Shelton JP, Sprenkle VL, Stevenson JW (2003) J Power Sources 113:1
110. Zhou XD, Anderson HU (2005) SOFC-IX: solid oxide fuel cells IX, electrochemical society proceedings. Quebec PQ, Canada, pp 1479–1486
111. Bongio EV, Black H, Raszewski FC, Edwards D, McConville CJ, Amarakoon VRW (2005) J Electroceram 14:193
112. Simner SP, Anderson MD, Pederson LR, Stevenson JW (2005) J Electrochem Soc 152:A1851
113. Coffey G, Hardy J, Marina O, Pederson L, Rieke P, Thomsen E (2004) Solid State Ionics 175:73
114. Simner S, Anderson M, Bonnett J, Stevenson J (2004) Solid State Ionics 175:79
115. Yokokawa H, Sakai H, Horita T, Yamaji K, Brito ME, Kishimoto H (2008) J Alloys Compd 452:41
116. Mai A, Haanappel VAC, Uhlenbruck S, Tietz F, Stöver D (2005) Solid State Ionics 176:1341
117. Mai A, Haanappel VAC, Tietz F, Stöver D (2005) Solid oxide fuel cells IX (SOFC IX). In: Singhal SC, Mizusaki J (eds) The electrochemical society. Pennington, USA, pp 1627–1635
118. Martínez-Amesti A, Larrañaga A, Rodríguez-Martínez LM, Aguayo AT, Pizarro JL, Nó ML, Laresgoiti A, Arriortua MI (2008) J Power Sources 185:401
119. Tsipis EV, Kharton VV (2008) J Solid State Electrochem 12:1039
120. Anderson MD, Stevenson JW, Simner SP (2004) J Power Sources 129:188
121. Simner SP, Schelton JP, Anderson MD, Stevenson JW (2003) Solid State Ionics 161:11
122. Bebelis S, Kournoutis V, Mai A, Tietz F (2008) Solid State Ionics 179:1080
123. Dusastre V, Kilner JA (1999) Solid State Ionics 126:163
124. Steele BCH (1996) Solid State Ionics 86–88:1223
125. Kindermann L, Dos D, Nickel H, Hilpert K, Appel CC, Poulsan FW (1997) J Electrochem Soc 144:717
126. Steele BCH (2000) Solid State Ionics 129:95
127. Kostogloudis GCh, Ftikos Ch (1999) Solid State Ionics 126:143
128. Haanappel VAC, Mertens J, Mai A (2006) J Fuel Cell Sci Technol 3:263
129. Uhlenbruck S, Moskalewicz T, Jordan N, Penkalla HJ, Buchkremer HP (2009) Solid State Ionics 180:418
130. Mai A, Becker M, Assenmacher W, Tietz F, Hathiramani D, Ivers-Tiffée E, Stöver D, Mader W (2006) Solid State Ionics 177:1965
131. Yokokawa H, Tu HY, Iwanschitz B, Mai A (2008) J Power Sources 182:400
132. Tietz F, Fu QX, Haanappel VAC, Mai A, Menzler NH, Uhlenbruck S (2007) Int J Appl Ceram Technol 4:436
133. Tietz F, Mai A, Stöver D (2008) Solid State Ionics 179:1509
134. Tietz F, Arul Raj I, Zahid M, Stöver D (2006) Solid State Ionics 177:1753
135. Meng XW, Lv SQ, Ji Y, Tao W, Zhang YL (2008) J Power Sources 183:581
136. Shao ZP, Haile SM (2004) Nature 431:170
137. Wei B, Lv Z, Huang XQ, Miao JP, Sha XQ, Xin XS, Su WH (2006) J Eur Ceram Soc 26:2827
138. Kharton VV, Yaremchenko AA, Kovalevsky AV, Viskup AP, Naumovich EN, Kerko PF (1999) J Membrane Sci 163:307
139. Tofan C, Klvana D, Kirchnerova J (2002) Appl Catal B 36:311
140. Gharbage B, Baker RT, Marques FMB (1998) J Mater Sci Lett 17:75
141. Khromushin IV, Aksenova TI, Zhotabaev ZhR (2003) Solid State Ionics 162–163:37
142. Hybbert DB (1993) In: Tejuca LG, Fierro JLG (eds) Properties and applications of perovskite-type oxides. Marcel Dekker, New York, pp 325–342
143. Carolan MF, Dyer PN, LaBar JM, Thorogood RM (1993) US Patent 5(240):473
144. Xia C, Lang Y, Meng G (2004) Fuel Cells 4:41
145. Yan AY, Cheng MJ, Dong YL, Yang WS, Maragou V, Song SQ, Tsiakaras P (2006) Appl Catal B 66:64
146. Zinkevich M, Aldinger F (2004) J Alloys Compd 375:147
147. Tsipis EV, Kiselev EA, Kolotygin VA, Waerenborgh JC, Cherepanov VA, Kharton VV (2008) Solid State Ionics 179:2170
148. Chiba R, Yoshimura F, Sakurai Y (1999) Solid State Ionics 124:281
149. Chiba R, Yoshimura F, Sakurai Y (2002) Solid State Ionics 152–153:575
150. Orui H, Watanabe K, Chiba R, Arakawa M (2004) J Electrochem Soc 151:A1412
151. Komatsu T, Arai H, Chiba R, Nozawa K, Arakawa M, Sato K (2006) Electrochem Solid-State Lett 9:A9
152. Komatsu T, Arai H, Chiba R, Nozawa K, Arakawa M, Sato K (2007) J Electrochem Soc 154:B379
153. Chiba R, Orui H, Komatsu T, Tabata Y, Nozawa K, Arakawa M, Sato K, Arai H (2008) J Electrochem Soc 155:B575
154. Kharton VV, Viskup AP, Marozau IP, Naumovich EN (2003) Mater Lett 57:3017
155. Tietz F, Raj IA, Zahid M, Mai A, Stöver D (2007) Prog Solid State Chem 35:539
156. Teraoka Y, Zhang HM, Okamoto K, Yamazoe N (1988) Mater Res Bull 23:51
157. Patrakeev MV, Bahteeva JA, Mitberg EB, Leonidov IA, Kozhevnikov VL, Poeppelmeier KR (2003) J Solid State Chem 172:219
158. Kindermann L, Poulsen FW, Larsen PH, Nickel H, Hilpert K (1998) In: Stevens P (ed), Proc. 3rd Eur. Forum on SOFC, Switzerland 2:123–132
159. Piao JH, Sun KN, Zhang NQ, Chen XB, Xu S, Zhou DR (2007) J Power Sources 172:633
160. Tai LW, Nasrallah MM, Anderson HU, Sparlin DM, Sehlin SR (1995) Solid State Ionics 76:259
161. Petric A, Huang P, Tietz F (2000) Solid State Ionics 135:719
162. Teraoka Y, Nobunaga T, Okamoto K, Miura N, Yamazoe N (1991) Solid State Ionics 48:207
163. Tai LW, Nasrallah MM, Anderson HU, Sparlin DM, Sehlin SR (1995) Solid State Ionics 76:273
164. Naumovich EN, Patrakeev MV, Kharton VV, Yaremechenko AA, Logvinovich DI, Marques FMB (2005) Solid State Sci 7:1353
165. Munnings CN, Skinner SJ, Amow G, Whitfiels PS, Davidson IJ (2005) Solid State Ionics 176:1895
166. Vashook VV, Ullmann H, Olshevskaya OP, Kulik VP, Lukashevich VE, Kokhanovskij LV (2000) Solid State Ionics 138:99
167. Al Daroukh M, Vashook VV, Ullmann H, Tietz F, Arual Raj I (2003) Solid State Ionics 158:141
168. Skinner SJ, Kilner JA (2000) Solid State Ionics 135:709
169. Zhao F, Wang XF, Wang ZY, Peng RR, Xia CR (2008) Solid State Ionics 179:1450
170. Aguadero A, Alonso JA, Esudero MJ, Daza L (2008) Solid State Ionics 179:393
171. Jin C, Liu J (2009) J Alloys Compd 474:573
172. Xia CR, Liu ML (2002) Adv Mater 14:521
173. Wang SR, Kato T, Nagata S, Honda T, Kaneko T, Iwashita N, Dokiya M (2002) Solid State Ionics 146:203
174. Liu Y, Mori M, Funahashi Y, Hirano A (2007) Electrochem Commun 9:1918
175. Sakito Y, Hirano A, Imanishi N, Takeda Y, Yamamoto O, Liu Y (2008) J Power Sources 182:476
176. Wang LS, Barnett SA (1995) Solid State Ionics 76:103

177. Sahibzada M, Benson SJ, Rudkin RA, Kilner JA (1995) Solid State Ionics 113–115:285
178. Haanappel VAC, Rutenbeck D, Mai A, Uhlenbruck S, Sebold D, Wesemeyer H, Röwekamp B, Tropartz C, Tietz F (2004) J. Power Sources 130:119
179. Sun CW, Xie Z, Xia CR, Li H, Chen LQ (2006) Electrochem Commun 8:833
180. Fukui T, Murata K, Ohara S, Abe H, Naito M, Nogi K (2004) J Power Sources 125:17
181. Abe H, Murata K, Fukui T, Moon WJ, Kaneko K, Naito M (2006) Thin Solid Films 496:49
182. Tanner CW, Fung KZ, Virkar AV (1997) J Electrochem Soc 144:21
183. Liu Y, Zha SW, Liu ML (2004) Adv Mater 16:256
184. Mamak M, Metraux GS, Petrov S, Coombs N, Ozin GA, Green MA (2003) J Am Chem Soc 125:5161
185. Leng YJ, Chan SH, Liu QL (2008) Int J Hydrogen Energy 33:3808
186. Antonietti M, Ozin GA (2004) Chem Eur J 10:28
187. Jiang SP (2006) Mater Sci Eng A 418:199
188. Huang Y, Vohs JM, Gorte RJ (2006) J Electrochem Soc 153:A951
189. Sholklapper TZ, Kurokawa H, Jacobson CP, Visco SJ, De Jonghe LC (2007) Nano Lett 7:2136
190. Huang KQ, Hou PY, Goodenough JB (2000) Solid State Ionics 129:237
191. Yang Z, Weil KS, Paxton DM, Stevenson JW (2003) J Electrochem Soc 150:A1188
192. Graham HC, Davis HH (1971) J Am Ceram Soc 54:89
193. Hilpert K, Das D, Miller M, Peck DH, Weiβ R (1996) J Electrochem Soc 143:3642
194. Konysheva E, Penkalla H, Wessel E, Mertens J, Seeling U, Singheiser L, Hilpert K (2006) J Electrochem Soc 153:A765
195. Badwal SPS, Deller R, Foger K, Ramprakash Y, Zhang JP (1997) Solid State Ionics 99:297
196. Paulson SC, Birss VI (2004) J Electrochem Soc 151:A1961
197. Jiang SP, Zhang S, Zhen YD (2006) J Electrochem Soc 153:A127
198. Jiang SP, Zhang JP, Foger K (2000) J Electrochem Soc 147:3195
199. Fergus JW (2007) Int J Hydrogen Energy 32:3664
200. Steinberger-Wilckens R, Blum L, Buchkremer H, Gross S, de Haart L, Hilpert K, Nabielek H, Quadakkers W, Reisgen U, Steinbrech RW, Tietz F (2006) Int J Appl Ceram Technol 3:470
201. Konycheva E, Hilpert K, Nabielek H, Steinberger-Wilckens R, Vinke IC, Wessel E, Zahid M (2005) Proceedings of the Fuel Cell Seminar. Palm Spring
202. Taniguchi S, Kadowaki M, Kawamura H, Yasuo T, Akiyama Y, Miyake Y, Saitoh T (1995) J Power Sources 55:73
203. Taniguchi S, Kadowaki M, Yasuo T, Akiyama Y, Itoh Y, Miyake Y, Nishio K (1996) Denki Kagaku 64:568
204. Gindorf C, Singheiser L, Hilpert K (2005) J Phys Chem Solids 66:384
205. Yokokawa H, Horita T, Sakai N, Yamaji K, Brito ME, Xiong YP, Kishimoto H (2006) Solid State Ionics 177:3193
206. Jiang SP, Zhang JP, Zheng XG (2002) J Eur Ceram Soc 22:361
207. Jiang SP, Zhang JP, Apateanu L, Foger K (2000) J Electrochem Soc 147:4013
208. Jiang SP, Zhang S, Zhen YD (2005) J Mater Res 20:747
209. Jiang SP, Zhen YD, Zhang S (2006) J Electrochem Soc 153: A1511
210. Zhen YD, Tok AIY, Boey FYC, Jiang SP (2008) Electrochem Solid-state Lett 11:B42
211. Jiang SP, Zhen YD (2008) Solid State Ionics 179:1459
212. Chen XB, Zhang L, Jiang SP (2008) J Electrochem Soc 155: B1093
213. Komatsu T, Chiba R, Arai H, Sato K (2008) J Power Sources 176:132
214. Kim JY, Canfield NL, Chick LA, Meinhardt KD, Sprenkle VL (2005) In Bansal NP (ed), Advances in solid oxide fuel cells: ceramic engineering and science proceedings. Wiley Publisher, Ohio, USA 26:129-138
215. Chen X, Hou PY, Jacobson CP, Visco SJ, De Jonghe LC (2005) Solid State Ionics 176:425
216. Kurokawa H, Jacobson CP, De Jonghe LC, Visco SJ (2007) Solid State Ionics 178:287
217. Yang ZG, Xia GG, Simner SP, Stevenson JW (2005) In Bansal NP (ed), Advances in solid oxide fuel cells: ceramic engineering and science proceedings. Wiley Publisher, Ohio, USA 26:201–208
218. Gannon PE, Gorokhovsky VI, Deibert MC, Smith RJ, Kayani A, White PT, Sofie S, Yang ZG, McCready D, Visco S, Jacobson C, Kurokawa H (2007) Int J Hydrogen Energy 32:3672
219. Gannon P, Deibert M, White P, Smith R, Chen H, Priyantha W, Lucas J, Gorokhovsky V (2008) Int J Hydrogen Energy 33:3991
220. Chu CL, Wang JY, Lee S (2008) Int J Hydrogen Energy 33:2536